

NON-UNIFORM QUANTUM FOURIER TRANSFORM

JUNAID AFTAB, YUEHAW KHOO, AND HAIZHAO YANG

ABSTRACT. The Discrete Fourier Transform (DFT) is central to the analysis of uniformly sampled signals, yet many practical applications involve non-uniform sampling, requiring the Non-Uniform Discrete Fourier Transform (NUDFT). While quantum algorithms for the standard DFT are well established, a corresponding framework for the non-uniform case remains underdeveloped. This work introduces a quantum algorithm for the Non-Uniform Quantum Fourier Transform (NUQFT) based on a low-rank factorization of the NUDFT matrix. The factorization is translated into an explicit quantum construction using block encodings, Quantum Signal Processing, and the Linear Combination of Unitaries framework, yielding an ϵ -accurate block encoding of the NUDFT matrix with controlled approximation error from both classical truncation and quantum implementation. Under standard oracle access assumptions for non-uniform sampling points, we derive explicit, non-asymptotic gate-level resource estimates. The resulting complexity scales polylogarithmically with target precision, quadratically with the number of qubits through the quantum Fourier transform, and logarithmically with a geometry-dependent conditioning parameter induced by the non-uniform grid. This establishes a concrete and resource-efficient quantum analogue of the NUDFT and provides a foundation for quantum algorithms on irregularly sampled data.

1. INTRODUCTION

The Discrete Fourier Transform (DFT), introduced by Gauss and later popularized by Cooley and Tukey [1], provides a fundamental framework for computing Fourier coefficients from uniformly sampled data and underpins applications in signal processing, data compression, and numerical solutions of differential equations (see, e.g., [2–4]). In practice, uniform sampling is often infeasible due to physical constraints, adaptive sampling, or irregular geometries. The Non-Uniform Discrete Fourier Transform (NUDFT) [5] generalizes the DFT to arbitrary sampling grids, enabling spectral analysis on non-uniform data and irregular computational domains, with important applications in imaging and numerical methods (see, e.g., [6, 7]). Consequently, a broad class of efficient classical algorithms for computing the NUDFT has been developed (see, e.g., [8–16]).

The Quantum Fourier Transform (QFT) (see, e.g., [17–19]) is the quantum analogue of the DFT and a central primitive in quantum algorithm design. It appears as a core subroutine in many quantum algorithms, including Shor’s factoring algorithm [20], Kitaev’s quantum phase estimation [21], quantum linear systems algorithms [22], ground-state energy estimation [23], and quantum arithmetic [24, 25]. Recent work has explored several extensions of the QFT, such as multi-dimensional extensions, approximate implementations with reduced gate complexity, topology-aware variants adapted to specific hardware architectures, and fault-tolerant constructions for error-corrected quantum computation (see, e.g., [26–31]). In contrast, quantum algorithms for Fourier transforms on non-uniform grids, particularly in a fully quantum setting, remain relatively underexplored.

In this work, we propose a quantum algorithm for the NUDFT, termed the Non-Uniform Quantum Fourier Transform (NUQFT). The construction builds on the low-rank matrix factorization framework of Antolín and Townsend [14] and translates this decomposition into an explicit quantum algorithm. The factorization is implemented using Quantum Signal Processing (QSP) [32, 33] together with the Linear Combination of Unitaries (LCU) [34] algorithms. This yields an explicit block encoding [33] of the NUDFT matrix to arbitrary precision, with controlled approximation

errors stemming from both the classical low-rank truncation and its quantum realization. Finally, we provide explicit gate-level resource estimates for the resulting circuits under standard oracle access assumptions for non-uniform sampling points.

1.1. Problem Statement. Let $\{x_j\}_{j=0}^{N-1} \subseteq \mathbb{C}$ denote samples taken at non-uniform locations $\{t_j\}_{j=0}^{N-1} \subseteq \mathbb{T}$, viewed as a discrete representation of an underlying function $f : \mathbb{T} \rightarrow \mathbb{C}$. The Non-Uniform Discrete Fourier Transform (NUDFT) of $\{x_j\}_{j=0}^{N-1}$, evaluated at non-uniform frequencies $\{\omega_k\}_{k=0}^{N-1} \subseteq \mathbb{R}$, is defined by

$$\begin{pmatrix} X_0 \\ X_1 \\ \vdots \\ X_{N-1} \end{pmatrix} = \begin{pmatrix} e^{-i\omega_0 t_0} & e^{-i\omega_0 t_1} & \dots & e^{-i\omega_0 t_{N-1}} \\ e^{-i\omega_1 t_0} & e^{-i\omega_1 t_1} & \dots & e^{-i\omega_1 t_{N-1}} \\ \vdots & \vdots & \ddots & \vdots \\ e^{-i\omega_{N-1} t_0} & e^{-i\omega_{N-1} t_1} & \dots & e^{-i\omega_{N-1} t_{N-1}} \end{pmatrix} \begin{pmatrix} x_0 \\ x_1 \\ \vdots \\ x_{N-1} \end{pmatrix} \quad (1)$$

In the literature, Equation (1) is known as the Type-III NUDFT, and the matrix is denoted by F_{III} . Two special cases arise depending on whether the sampling locations and frequency points are uniform or non-uniform:

- (I) **Type-I NUDFT.** The sequence $\{t_j\}_{j=0}^{N-1}$ is sampled uniformly at points $t_j = 2\pi j/N$, but the sequence $\{\omega_k\}_{k=0}^{N-1}$ is sampled at potentially non-uniform points. We denote the corresponding matrix as F_{I} .
- (II) **Type-II NUDFT.** The sequence $\{t_j\}_{j=0}^{N-1}$ is sampled at potentially non-uniform points $\{t_j\}_{j=0}^{N-1}$, but sequence $\{\omega_k\}_{k=0}^{N-1}$ is uniformly space with $\omega_k = k$ for $k = 0, \dots, N-1$. We denote the corresponding matrix as F_{II} .

We argue in Section 3 that it suffices to develop a quantum algorithm for the Type-II case.

1.2. Summary of Results. Let $N = 2^n$ for some $n \geq 1$. Antolín and Townsend in [14] approximate a Type-II NUDFT matrix, denoted by F_{II} , by an expression of the form $F_{\text{II}} \approx \sum_{r=0}^{K-1} D_{\vec{u}_r} F D_{\vec{v}_r}$. See Section 3 for the more general form of F_{II} that needs to be considered. Here, F denotes the standard discrete Fourier transform matrix, and $D_{\vec{u}_r}$ and $D_{\vec{v}_r}$ are diagonal matrices. Under the standard assumption of oracle access to the sampling points $\{t_j\}_{j=0}^{2^n-1}$, our algorithm constructs quantum circuits $U_{\vec{u}_r}$ and $U_{\vec{v}_r}$ that yield block encodings of $D_{\vec{u}_r}$ and $D_{\vec{v}_r}$, respectively. By combining these block-encoded diagonal operators with the standard block encoding of F and applying the Linear Combination of Unitaries (LCU) technique, our algorithm implements the operator $\sum_{r=0}^{K-1} D_{\vec{u}_r} F D_{\vec{v}_r}$. Our results include non-asymptotic gate-count estimates (Theorem 21), resource bounds for achieving ϵ -accurate block encodings (Theorem 25), and simplified complexity estimates (Corollary 26). We present explicit gate-count estimates sufficient to obtain an ϵ -accurate block encoding.

Result 1 (Asymptotic Version of Theorem 21 based on Corollary 26). Let $\epsilon > 0$ and let $n \in \mathbb{N}$ with $N = 2^n$. There exists a quantum circuit, V_{II} , that implements an ϵ -accurate block-encoding of F_{II} . Let

$$L_{n,\epsilon} := n + \log(1/\epsilon), \quad \kappa := \max_j (1 + (y_j^*)^2)^{-1/2}, \quad (2)$$

where $y_j^* \in (-1, 1)$ are points determined by the non-uniform sampling points. The circuit uses $\mathcal{O}(L_{n,\epsilon} + \log(1 + \kappa L_{n,\epsilon}))$ qubits, $\mathcal{O}(n + \log L_{n,\epsilon})$ Hadamard gates, $\mathcal{O}(L_{n,\epsilon}^2 + \log(1 + \kappa L_{n,\epsilon}))$ CNOT gates, $\mathcal{O}(L_{n,\epsilon} + \log(1 + \kappa L_{n,\epsilon}))$ Toffoli and σ_X gates, and $\mathcal{O}(n^2 + L_{n,\epsilon}^2 + \log(1 + \kappa L_{n,\epsilon}))$ single-qubit controlled rotation gates. The circuit depth is $\mathcal{O}(L_{n,\epsilon} \log L_{n,\epsilon} + \log(1 + \kappa L_{n,\epsilon}))$.

The resource bounds in Result 1 depend on three parameters: the number of qubits n , the target accuracy ϵ , and the geometry-dependent quantity κ . The dependence on the accuracy parameter enters solely through the logarithmic factor $\log(1/\epsilon)$, which appears additively with n in

the composite parameter $L_{n,\epsilon}$. Consequently, increasing the target precision affects the overall gate counts and circuit depth only polylogarithmically. The quadratic dependence on n arises from the implementation of the quantum Fourier transform. All remaining gate counts scale as $L_{n,\epsilon} \log L_{n,\epsilon}$, with the exception of a single $L_{n,\epsilon}^2$ term, up to additional logarithmic factors depending on κ . The parameter κ , which captures the conditioning induced by the non-uniform sampling points, contributes only through logarithmic factors of the form $\log(1 + \kappa L_{n,\epsilon})$. In particular, no resource exhibits polynomial dependence on κ , and its effect remains subdominant whenever κ grows at most exponentially in n or $\log(1/\epsilon)$.

1.3. Related Works. In contrast to the extensive literature on the QFT, little work has addressed quantum implementations of Fourier transforms on non-uniform grids. To the best of our knowledge, the closest related proposal is due to Gyongyosi and Imre [35]. That work introduces a method termed ‘‘Quantum-SVD,’’ in which a standard QFT on a uniform grid is followed by a classical singular value decomposition–based interpolation step to approximate Fourier coefficients at non-uniform sampling points. As a result, the procedure is hybrid: the Fourier transform is quantum, while the handling of non-uniformity is performed classically. By contrast, the approach developed here provides a fully quantum implementation based on a block-encoding framework. Our work can also be placed in the broader context of efforts to develop circuit-level quantum analogues of classical integral transforms, including the quantum wavelet transform [36, 37], quantum Laplace transform [38, 39], quantum Hilbert transform [40, 41], quantum cosine transform [42, 43], quantum Chebyshev transform [44], and quantum Hermite transform [45].

1.4. Organization. The remainder of this paper is organized as follows. Section 2 reviews the necessary preliminaries, including the discrete and quantum Fourier transforms, as well as other quantum algorithmic primitives relevant to this study. Section 3 reviews the low-rank matrix factorization approach to the non-uniform discrete Fourier transform. Section 4 presents our quantum algorithm, and Section 5 provides the corresponding error analysis. Finally, Section 6 offers concluding remarks and discusses potential directions for future work.

Acknowledgments. J. Aftab was supported by NSF DMS-2231533. Y. Khoo was partially funded by NSF DMS-2339439, DOE DE-SC0022232, DARPA The Right Space HR0011-25-9-0031, and a Sloan research fellowship. H. Yang was partially supported by the US National Science Foundation under awards IIS-2520978, GEO/RISE-5239902, the Office of Naval Research Award N00014-23-1-2007, DOE (ASCR) Award DE-SC0026052, and the DARPA D24AP00325-00. Approved for public release; distribution is unlimited.

2. PRELIMINARIES

This section presents the necessary preliminary material. Section 2.1 introduces the notation used throughout the paper. Section 2.2 reviews the Quantum Fourier Transform (QFT). Finally, Section 2.3 summarizes the quantum algorithmic primitives that form the foundation of the proposed method.

2.1. Notation. We briefly discuss the main notation used throughout this work.

2.1.1. Standard Notation. Let \mathbb{R} , \mathbb{C} , and \mathbb{N} denote the sets of real, complex and natural numbers, respectively. Let \mathbb{T} denote the 1-dimensional torus (i.e., the unit circle) identified with the interval $[0, 1]$ with its endpoints identified. If $f, g : \mathbb{N} \rightarrow \mathbb{R}^+$ are non-negative functions, we use the following standard notation from complexity theory:

- (1) $f(n) = \mathcal{O}(g(n))$ if and only if there exists a constant $C > 0$ and an integer $N \in \mathbb{N}$ such that $f(n) \leq Cg(n)$ for all $n \geq N$.
- (2) $f(n) = \Omega(g(n))$ if and only if there exists a constant $C > 0$ and an integer $N \in \mathbb{N}$ such that $f(n) \geq Cg(n)$ for all $n \geq N$.

(3) $f(n) = \Theta(g(n))$ if and only if $f(n) = \mathcal{O}(g(n))$ and $f(n) = \Omega(g(n))$.

For $r \in \mathbb{N} \cup \{0\}$, $T_r(x)$ denotes the degree- r Chebyshev polynomial of the first-kind on $[-1, 1]$ defined recursively by $T_0(x) = 1$, $T_1(x) = x$ and

$$T_r(x) = 2xT_{r-1}(x) - T_{r-2}(x), \quad r \geq 2. \quad (3)$$

Similarly, $S_r(x)$ denotes the degree- r Chebyshev polynomial of the second-kind on $[-1, 1]$ defined recursively by $S_0(x) = 1$, $S_1(x) = 2x$ and

$$S_r(x) = 2xS_{r-1}(x) - S_{r-2}(x), \quad r \geq 2. \quad (4)$$

2.1.2. Linear Algebra Notation. Vectors in \mathbb{R}^n or \mathbb{C}^n are denoted by lowercase Roman letters with an overhead arrow. The linear algebra notation used throughout this paper is summarized below:

- (1) $\|\vec{x}\|_1$ denotes the 1-norm of a vector \vec{x} . Similarly, $\|\vec{x}\|_\infty$ denotes the ∞ -norm of \vec{x} .
- (2) $\|A\|$ denotes the spectral norm of a matrix A , defined as its largest singular value.
- (3) $\|A\|_{\max}$ denotes the maximum absolute value among the entries of A .
- (4) The symbol \circ denotes the elementwise (Hadamard) product, acting entry-wise on vectors or matrices of the same dimensions.
- (5) If \vec{x} is a vector and f is a function, then $f(\vec{x})$ denotes the componentwise application of f to \vec{x} .

2.1.3. Quantum Computing Notation. A single-qubit quantum state is represented by a unit vector in \mathbb{C}^2 . In Dirac's notation, such a state is written as $|v\rangle$ and referred to as a *ket*, while its conjugate transpose, denoted $\langle v|$, is called a *bra*. A single-qubit quantum gate is a unitary operator in $\mathbb{C}^{2 \times 2}$. Common examples of single-qubit quantum gates include the Pauli matrices:

$$\sigma_X = \begin{pmatrix} 0 & 1 \\ 1 & 0 \end{pmatrix}, \quad \sigma_Y = \begin{pmatrix} 0 & -i \\ i & 0 \end{pmatrix}, \quad \sigma_Z = \begin{pmatrix} 1 & 0 \\ 0 & -1 \end{pmatrix}. \quad (5)$$

Single-qubit rotation gates about the X , Y , and Z axes are defined as follows:

$$e^{-i\theta\sigma_X} = \begin{pmatrix} \cos \theta & -i \sin \theta \\ -i \sin \theta & \cos \theta \end{pmatrix}, \quad e^{-i\theta\sigma_Y} = \begin{pmatrix} \cos \theta & -\sin \theta \\ \sin \theta & \cos \theta \end{pmatrix}, \quad e^{-i\theta\sigma_Z} = \begin{pmatrix} e^{-i\theta} & 0 \\ 0 & e^{i\theta} \end{pmatrix}. \quad (6)$$

We also denote the quantum gates $e^{-i\theta\sigma_X}$, $e^{-i\theta\sigma_Y}$, and $e^{-i\theta\sigma_Z}$ as $R_X(\theta)$, $R_Y(\theta)$, and $R_Z(\theta)$, respectively. Another important example of a single-qubit gate is the Hadamard gate:

$$H = \frac{1}{\sqrt{2}} \begin{pmatrix} 1 & 1 \\ 1 & -1 \end{pmatrix} = \text{---} \boxed{H} \text{---} \quad (7)$$

A k -qubit quantum state is a unit vector \mathbb{C}^{2^k} and a k -qubit quantum gate is a unitary operator in $\mathbb{C}^{2^k \times 2^k}$. An important example of a k -qubit gate is the k -fold tensor product of Hadamard gates:

$$H^{\otimes k} = \frac{1}{\sqrt{2}} \begin{pmatrix} 1 & 1 \\ 1 & -1 \end{pmatrix}^{\otimes k} = \text{---} \boxed{H^{\otimes k}} \text{---} \quad (8)$$

It is often necessary to construct multi-qubit controlled gates. A generic k -qubit gate, U , controlled on l qubits, is denoted as follows:

$$C^l U = \text{---} \overset{l}{\overbrace{\text{---}}} \text{---} \text{---} \boxed{U} \text{---} \overset{k}{\overbrace{\text{---}}} \text{---} \quad (9)$$

An important example of a two-qubit gate is the CNOT gate, while a three-qubit example is the Toffoli (CCNOT) gate:

$$\text{CNOT} = \begin{pmatrix} 1 & 0 & 0 & 0 \\ 0 & 1 & 0 & 0 \\ 0 & 0 & 0 & 1 \\ 0 & 0 & 1 & 0 \end{pmatrix} = \begin{array}{c} \text{---} \\ \bullet \\ \text{---} \\ \oplus \end{array} \quad \text{CCNOT} = \begin{pmatrix} 1 & 0 & 0 & 0 & 0 & 0 & 0 & 0 \\ 0 & 1 & 0 & 0 & 0 & 0 & 0 & 0 \\ 0 & 0 & 1 & 0 & 0 & 0 & 0 & 0 \\ 0 & 0 & 0 & 1 & 0 & 0 & 0 & 0 \\ 0 & 0 & 0 & 0 & 1 & 0 & 0 & 0 \\ 0 & 0 & 0 & 0 & 0 & 1 & 0 & 0 \\ 0 & 0 & 0 & 0 & 0 & 0 & 0 & 1 \\ 0 & 0 & 0 & 0 & 0 & 0 & 1 & 0 \end{pmatrix} = \begin{array}{c} \text{---} \\ \bullet \\ \text{---} \\ \text{---} \\ \bullet \\ \text{---} \\ \oplus \end{array} \quad (10)$$

Note that $\text{CNOT} = C\sigma_X$ and $\text{CCNOT} = C^2\sigma_X$. Single-qubit controlled rotations also play an important role in quantum computation. In particular, the following controlled rotation operation arises in the implementation of the Quantum Fourier Transform.

$$CR_m = \begin{pmatrix} 1 & 0 & 0 & 0 \\ 0 & 1 & 0 & 0 \\ 0 & 0 & 1 & 0 \\ 0 & 0 & 0 & e^{-2\pi i/2^m} \end{pmatrix} = \begin{array}{c} \text{---} \\ \bullet \\ \text{---} \\ \boxed{R_m} \end{array} \quad (11)$$

2.2. Quantum Fourier Transform. Let $N \in \mathbb{N}$. The Discrete Fourier Transform (DFT) can be interpreted as the linear map $\text{DFT}_N : \mathbb{C}^N \rightarrow \mathbb{C}^N$ given by the matrix whose (j, k) -entry is

$$(\text{DFT}_N)_{jk} = \frac{1}{\sqrt{N}} \omega_N^{jk}, \quad (12)$$

where $\omega_N = e^{-2\pi i/N}$ is a primitive N -th root of unity and $0 \leq j, k \leq N-1$. It is straightforward to verify that DFT_N is a unitary operator. The Quantum Fourier Transform (QFT) is the quantum analogue of the Discrete Fourier Transform and acts on quantum states by implementing DFT_N as a quantum circuit, denoted by U_{QFT} . The algorithm realizes U_{QFT} through a sequence of single-qubit and two-qubit gates based on the following expression:

$$U_{\text{QFT}} |x\rangle = \frac{1}{\sqrt{N}} \sum_{y=0}^{N-1} e^{-2\pi i xy/N} |y\rangle = \frac{1}{\sqrt{N}} \bigotimes_{\ell=0}^{n-1} \left(|0\rangle + e^{-2\pi i \sum_{m=1}^{n-\ell} x_{n-\ell-m}/2^m} |1\rangle \right). \quad (13)$$

The tensor-product form in Equation (13) is important because it reveals a hierarchical dependence: the last output qubit depends on all n input qubits, while earlier outputs depend on progressively fewer qubits. This structure enables a simplified and more efficient circuit implementation. In each of the n iterations in Algorithm 1, a Hadamard gate is applied followed by progressively fewer controlled phase rotations, giving a total of $\mathcal{O}(n^2)$ quantum gates. For a vector of size $N = 2^n$, the QFT has computational complexity $\mathcal{O}(\log^2 N) = \mathcal{O}(n^2)$, offering an exponential speedup over the classical FFT, which requires $\mathcal{O}(N \log N) = \mathcal{O}(n2^n)$ operations.

Algorithm 1: Quantum Fourier Transform (QFT) on an n -qubit register

Input: n -qubit quantum state $|x\rangle = |x_0 x_1 \cdots x_{n-1}\rangle$

Output: QFT-transformed quantum state $U_{\text{QFT}} |x\rangle$

for $\ell \leftarrow 0$ **to** $n-1$ **do**

| Apply Hadamard gate H to qubit $n-\ell$

| **for** $m \leftarrow 2$ **to** $n-\ell$ **do**

| | Apply CR_m (Equation (11)) with qubit $n-\ell-m$ (control) and qubit $n-\ell$ (target)

return QFT transformed quantum state $U_{\text{QFT}} |x\rangle$

2.3. Quantum Algorithm Primitives. We review the fundamental algorithmic primitives in quantum computation that underpin this work. In particular, we cover quantum arithmetic, the block encoding framework, quantum signal processing (QSP), and the Linear Combination of Unitaries (LCU) algorithm.

2.3.1. Quantum Arithmetic. We assume that all quantum algorithms take as input a fixed-precision binary number stored in an n -qubit quantum register, denoted $|x\rangle$. The leftmost m qubits encode the integer part, while the remaining $n - m$ qubits encode the fractional part. When necessary, an additional qubit may be introduced to represent the sign of the number. Formally,

$$|x\rangle = |x^{(m-1)}\rangle \otimes \cdots \otimes |x^{(0)}\rangle \otimes |x^{(-1)}\rangle \otimes \cdots \otimes |x^{(m-n)}\rangle, \quad (14)$$

where each $x^{(j)} \in \{0, 1\}$ and the number is represented as

$$x = \underbrace{\sum_{j=0}^{m-1} x^{(j)} 2^j}_{\text{integer part}} + \underbrace{\sum_{j=-1}^{-(n-m)} x^{(j)} 2^j}_{\text{fractional part}}. \quad (15)$$

Quantum algorithms for addition (see, e.g., [24, 46, 47]) and multiplication (see, e.g., [48–50]) have been extensively studied, with circuit complexities of $\mathcal{O}(n)$ for addition and $\mathcal{O}(n^2)$ for multiplication, measured in Toffoli and CNOT gates. Since the NUQFT algorithm considered here has overall complexity $\Omega(n^2)$, it is sufficient to treat addition and multiplication as elementary primitives. See Figure 1 for a quantum oracle U_{AM} that implements both addition and multiplication within a single quantum circuit.

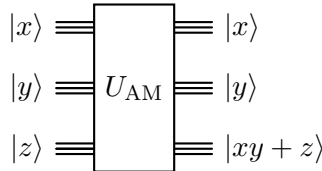


FIGURE 1. Quantum oracle for multiplication and addition implementing $|x\rangle|y\rangle|z\rangle \mapsto |x\rangle|y\rangle|xy + z\rangle$.

Recent work by Burge et al. [51] introduces a reversible quantum algorithm for computing the arcsine function using a quantum adaptation of the CORDIC (COordinate Rotation DIgital Computer) method. The algorithm iteratively approximates $\arcsin(x)$ through a sequence of reversible rotations, enabling efficient implementation on quantum hardware. For a p -bit output, it requires $\mathcal{O}(p)$ qubits and $\mathcal{O}(p^2)$ CNOT gates, with circuit depth scaling as $\mathcal{O}(p \log p)$, and achieves a worst-case approximation error of $\mathcal{O}(2^{-p})$.

2.3.2. Block Encoding. Quantum algorithms for matrix manipulation often assume that a potentially non-unitary matrix can be embedded as a block within a unitary matrix. The block-encoding framework provides a systematic approach for performing linear algebraic operations on a quantum computer. The key idea is to represent a subnormalized, possibly non-unitary matrix A/α as the upper-left block of a unitary matrix. Importantly, the block encoding need not be exact, motivating the following formal definition:

Definition 2. Let $\alpha, \epsilon \in \mathbb{R}^+$. Given $A \in \mathbb{C}^{r \times c}$, we say $U \in \mathbb{C}^{d \times d}$ for $d \geq \max\{r, c\}$ is a (α, ϵ) block encoding of A

$$\|A - \alpha(B_L^\dagger U B_R)\| \leq \epsilon, \quad (16)$$

where $B_L \in \mathbb{C}^{d \times r}$ and $B_R \in \mathbb{C}^{d \times c}$ are the first r and c columns of the identity matrix, respectively.

We will often consider d , r , and c as powers of two. In this case, if $A \in \mathbb{C}^{2^m \times 2^n}$, we will say that a unitary $U \in \mathbb{C}^{2^{m+a} \times 2^{n+a}}$ is a (α, a, ϵ) -block-encoding of A if

$$\|A - \alpha(\langle 0|^a \otimes I_{2^n})U(|0\rangle^a \otimes I_{2^m})\| \leq \epsilon \quad (17)$$

In most cases, we have $m = n$, and this is the case that will be considered below. For ease of notation, we write:

$$U = \begin{pmatrix} A/\alpha & * \\ * & * \end{pmatrix} \quad (18)$$

Let us consider an explicit computation to clarify the notation. Let $A \in \mathbb{C}^{2 \times 2}$ and $\alpha = 1$. In this case, we have

$$(\langle 0| \otimes I_2)U(|0\rangle \otimes I_2) = (I_2 \quad 0) \begin{pmatrix} A & C \\ B & D \end{pmatrix} \begin{pmatrix} I_2 \\ 0 \end{pmatrix} = (I_2 \quad 0) \begin{pmatrix} A \\ B \end{pmatrix} = A. \quad (19)$$

The case when $A \in \mathbb{C}^{2^s \times 2^s}$ for $s > 1$ and $a > 1$ is similar to the above. We will use the following lemma concerning block-encoding products of matrices in our analysis.

Lemma 3 (Lemma 53 in [33]). *If U is an (α, a, δ) -block-encoding of an s -qubit operator A , and V is a (β, b, ϵ) -block-encoding of an s -qubit operator B , then $(I_b \otimes U)(I_a \otimes V)$ is an $(\alpha\beta, a+b, \alpha\epsilon + \beta\delta)$ -block-encoding of AB , where I_a and I_b act on the ancilla qubits of U and V respectively.*

We will also use a result on block-encoding sparse matrices, which can be found in [33, Lemma 48]. For our purposes, it suffices to restrict attention to the case in which A is a sparse 0–1 matrix. The corresponding specialization of this result is stated below.

Lemma 4. *Let $A \in \mathbb{C}^{2^n \times 2^n}$ be a d_r -row-sparse and d_c -column-sparse 0-1 matrix. Suppose that we have access to the following $2(n+1)$ -qubit oracles:*

$$O_r : |i\rangle|k\rangle \mapsto |i\rangle|r_{ik}\rangle, \quad 0 \leq i < 2^n, \quad 0 \leq k < d_r, \quad (20)$$

$$O_c : |l\rangle|j\rangle \mapsto |c_{lj}\rangle|j\rangle, \quad 0 \leq j < 2^n, \quad 0 \leq l < d_c, \quad (21)$$

where r_{ik} is the index of the k -th non-zero entry of the i -th row of A , or if there are fewer than k non-zero entries, then $r_{ik} = k + 2^n$, and similarly c_{lj} is the index of the l -th non-zero entry of the j -th column of A , or if there are fewer than l non-zero entries, then $c_{lj} = l + 2^n$. Additionally, assume we have access to a one-bit oracle

$$O_A : |i\rangle|j\rangle|0\rangle \mapsto |i\rangle|j\rangle|A_{ij}\rangle, \quad 0 \leq i, j < 2^n, \quad (22)$$

where $A_{ij} \in \{0, 1\}$. Then one can implement a $(\sqrt{d_r d_c}, n+3, 0)$ -block-encoding of A with a single use of O_r, O_c , two uses of O_A and additionally $\mathcal{O}(n)$ one-qubit and two-qubit gates, while using $\mathcal{O}(1)$ ancilla qubits (which are discarded before the ϵ -post-selection step).

The proof of Lemma 4 follows the same argument as that of the general result in [33, Lemma 48] and is therefore omitted.

2.3.3. Quantum Signal Processing. Quantum signal processing (QSP) is a framework for implementing polynomial transformations of scalars that are block-encoded in a unitary operator. In particular, QSP constructs 2×2 unitary matrices whose entries are complex polynomials of a real scalar $x \in [-1, 1]$ by composing single-qubit rotations and phase gates. It considers a single-qubit unitary operator that block-encodes $x \in [-1, 1]$ as follows:

$$e^{i \arccos(x) \sigma_X} = \begin{pmatrix} x & i\sqrt{1-x^2} \\ i\sqrt{1-x^2} & x \end{pmatrix}, \quad \theta \in [0, \pi]. \quad (23)$$

For $\varphi = (\varphi_0, \dots, \varphi_\ell)$, QSP implements the following quantum circuit:

$$V_\varphi(x) = e^{i\varphi_0 \sigma_Z} e^{i \arccos(x) \sigma_X} e^{i\varphi_1 \sigma_Z} e^{i \arccos(x) \sigma_X} \dots e^{i \arccos(x) \sigma_X} e^{i\varphi_\ell \sigma_Z}. \quad (24)$$

Polynomial functions realizable by Equation (24) are completely characterized by the following result:

Proposition 5 (Theorem 3 in [33]). *Let $\ell \in \mathbb{N}$ and $x \in [-1, 1]$. There exists $\varphi = (\varphi_0, \varphi_1, \dots, \varphi_\ell) \in \mathbb{R}^{\ell+1}$ such that*

$$V_\varphi(x) = e^{i\varphi_0\sigma_Z} \prod_{j=1}^{\ell} \left(e^{i\arccos(x)\sigma_X} e^{i\varphi_j\sigma_Z} \right) = \begin{pmatrix} p(x) & iq(x)\sqrt{1-x^2} \\ iq^*(x)\sqrt{1-x^2} & p^*(x) \end{pmatrix} \quad (25)$$

if and only if $p, q \in \mathbb{C}[x]$ such that:

- (i) $\deg(p(x)) \leq \ell$ and $\deg(q(x)) \leq \ell - 1$,
- (ii) $p(x)$ has parity $\ell \pmod{2}$ and $q(x)$ has parity $\ell - 1 \pmod{2}$ ¹,
- (iii) For all $x \in [-1, 1]$, we have $|p(x)|^2 + (1-x^2)|q(x)|^2 = 1$.

Example 6. QSP is an important quantum circuit because it enables the implementation of various polynomial transformations. A simple choice of phase factors $(0, \dots, 0) \in \mathbb{R}^{\ell+1}$ ensures that $p(x) = T_\ell(x)$, where $T_\ell(x)$ is the degree- ℓ Chebyshev polynomial of the first kind. We will use this result below. This observation has also recently been used to advocate QSP as a framework for function approximation (see, e.g., [52, 53]).

3.3.4. Linear Combination of Unitaries. The Linear Combination of Unitaries (LCU) algorithm [54] provides a framework for implementing a linear combination of unitary operators on a quantum computer. Let $M \in \mathbb{N}$, and let $\alpha_1, \dots, \alpha_M \in \mathbb{R}$ and U_1, \dots, U_M be k -qubit unitary operators. The LCU method aims to implement the operator $U = \sum_{j=1}^M \alpha_j U_j$. The algorithm assumes that the following two operators can be implemented. First, it assumes the existence of a state preparation (PREP) oracle:

$$\text{PREP} |0\rangle = \frac{1}{\sqrt{\|\vec{\alpha}\|_1}} \sum_{j=1}^M \sqrt{\alpha_j} |j\rangle, \quad (26)$$

where $\sqrt{\cdot}$ denotes the principal branch of the square root. Second, it assumes that a multi-qubit controlled gate, also called a select (SEL) oracle in the literature, can be implemented:

$$\text{SEL} = \sum_{j=1}^M U_j \otimes |j\rangle\langle j|. \quad (27)$$

can be implemented. Assuming access to the required operators, the LCU algorithm implements the unitary operator $U_{\text{LCU}} = \text{PREP}^\dagger \cdot \text{SEL} \cdot \text{PREP}$. See Figure 2 for the corresponding quantum circuit. If $|\psi\rangle$ denotes a k -qubit input state, $|0\rangle^{\log M}$ represents $\mathcal{O}(\log M)$ ancilla qubits, we have

$$U_{\text{LCU}} |\psi\rangle |0\rangle^{\log M} = \frac{1}{\|\vec{\alpha}\|_1} \left(\sum_{j=1}^M \alpha_j U_j \right) |\psi\rangle |0\rangle^{\log M} + |\perp\rangle, \quad (28)$$

where $|\perp\rangle$ denotes a potentially non-normalized state satisfying $(I_{2^k} \otimes |0\rangle^{\log M} \langle 0|^{\log M}) |\perp\rangle = 0$. Note that the LCU algorithm implements a $(\|\vec{\alpha}\|_1, \log M, 0)$ -block-encoding of $\sum_{j=1}^M \alpha_j U_j$.

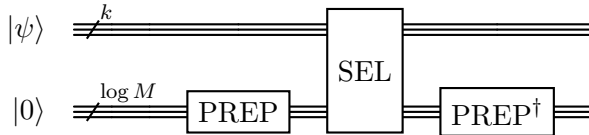


FIGURE 2. Quantum circuit U_{LCU} implementing the LCU algorithm.

¹A polynomial is said to have parity zero (one) if it is an even (odd) polynomial.

3. CLASSICAL ALGORITHM FOR NON-UNIFORM DISCRETE FOURIER TRANSFORM

In this section, we review a classical algorithm for the nonuniform discrete Fourier transform based on a low-rank matrix factorization approach, as presented in [14].

3.1. Type-II NUDFT. We first present the algorithm for the Type-II NUDFT, which assumes uniform frequency points given by $\omega_k = k$ for $k = 0, \dots, N - 1$.

3.1.1. Perturbed Equispaced Grid Setting. We begin by describing the algorithm in the special case where the nonuniform grid points are obtained by perturbing an equispaced grid. WLOG, let $\{t_j\}_{j=0}^{N-1} \subseteq [0, 1)$ such that²

$$\left| t_j - \frac{j}{N} \right| \leq \frac{\gamma}{N}, \quad (29)$$

for some $\gamma \in [0, 1/2]$. The simple but important observation is that the entries of F_{II} can be written as

$$(F_{\text{II}})_{jk} = e^{-2\pi i t_j k} = e^{-2\pi i (t_j - \frac{j}{N})k} e^{-2\pi i \frac{jk}{N}}, \quad (30)$$

for $0 \leq j, k \leq N - 1$. This observation leads to the matrix decomposition

$$F_{\text{II}} = A \circ F, \quad (31)$$

where F is the DFT matrix, and the entries of A are given by $A_{jk} = e^{-2\pi i (t_j - j/N)k}$. The matrix A is defined by sampling the bivariate function $(x, y) \mapsto e^{-2\pi i xy}$ over the domain $[-\gamma/N, \gamma/N] \times [0, N]$. As shown in [14], the construction of a low-rank factorization of A is based on approximating this function by a bivariate polynomial of degree $(K - 1)$, which can then be extended to obtain a rank- K approximation of A . This polynomial approximation is derived from a truncated Chebyshev expansion of e^{-ixy} [14, Appendix A]. As a result, the resulting rank- K approximation of A takes the form

$$A_K = \sum_{r=0}^{K-1}' \underbrace{\left[\sum_{q=0}^{K-1}' \alpha_{qr} \left(\exp(-i\pi N(\vec{t} - \vec{e})) \circ T_p \left(\frac{N(\vec{t} - \vec{e})}{\gamma} \right) \right) \right]}_{\vec{u}_r} \underbrace{T_r \left(\frac{2\vec{\omega}^\top}{N} - \vec{1}^\top \right)}_{\begin{cases} 2\vec{v}_r^\top & r = 0 \\ \vec{v}_r^\top & r \geq 1. \end{cases}} \quad (32)$$

Here $\vec{e} = (0, \frac{1}{N}, \dots, \frac{N-1}{N})^\top$, $\vec{\omega} = (0, 1, \dots, N-1)^\top$, and the primes on the summands indicate that the first term should be halved. The coefficients α_{qr} are given by

$$\alpha_{qr} = \begin{cases} 4i^r J_{\frac{q+r}{2}}(-\gamma\pi/2) J_{\frac{r-q}{2}}(-\gamma\pi/2), & \text{if } \text{mod}(|q - r|, 2) = 0, \\ 0, & \text{otherwise} \end{cases} \quad (33)$$

where $J_\nu(\cdot)$ denotes the Bessel function of the first kind of order ν . In order to eliminate the primes in the summand, we define a new quantity α'_{qr} , which will replace α_{qr} in subsequent expressions.

$$\alpha'_{qr} = \begin{cases} \frac{1}{4} \alpha_{qr} & \text{if } q = r = 0, \\ \frac{1}{2} \alpha_{qr} & \text{if } q = 0, r \neq 0 \text{ or } r = 0, q \neq 0, \\ \alpha_{qr} & \text{otherwise} \end{cases} \quad (34)$$

The analysis in [14] shows that it suffices to choose $K = \mathcal{O}\left(\frac{\log(1/\epsilon'_{\text{trunc}})}{\log \log(1/\epsilon'_{\text{trunc}})}\right)$ to ensure that the approximation satisfies $\|A - A_K\|_{\max} \leq \epsilon'_{\text{trunc}}$ for some $\epsilon'_{\text{trunc}} > 0$. Consequently, the matrix F_{II}

²We can compensate for this by introducing a factor of 2π in the complex exponential.

can then be approximated as

$$F_{\text{II}} = (A \circ F) \approx (A_K \circ F) = \sum_{r=0}^{K-1} D_{\vec{u}_r} F D_{\vec{v}_r}, \quad (35)$$

where $D_{\vec{u}_r} = \text{diag}(\vec{u}_r)$ and $D_{\vec{v}_r} = \text{diag}(\vec{v}_r)$. Since the complexity of applying the DFT matrix, F , is $\mathcal{O}(N \log N)$, the overall complexity of implementing the Type-II NUDFT in the special case where the non-uniform grid points $\{t_j\}_{j=0}^{N-1} \subseteq [0, 1]$ are generated by perturbing an equispaced grid is

$$\mathcal{O}\left(\frac{N \log N \log(1/\epsilon'_{\text{trunc}})}{\log \log(1/\epsilon'_{\text{trunc}})}\right). \quad (36)$$

3.1.2. General Nonuniform Node Distribution. We now discuss how to implement the Type-II NUDFT when the nodes $\{t_j\}_{j=0}^{N-1} \subseteq [0, 1]$ are distributed arbitrarily. The key idea is to reduce the problem to the equispaced case considered previously by identifying a sequence $\{s_j\}_{j=0}^{N-1} \subseteq \{0, \dots, N-1\}$ such that

$$s_j = \begin{cases} m & \text{if } |t_j - \frac{m}{N}| \leq 1/2N \text{ and } m \neq N, \\ 0 & \text{if } |t_j - 1| \leq 1/2N. \end{cases} \quad (37)$$

Note that s_n/N is the closest point to t_j on the equidistant grid $\{0, 1/N, \dots, (N-1)/N\} \subseteq [0, 1]$. We have

$$(F_{\text{II}})_{j,k} = e^{-2\pi i t_j k} = e^{-2\pi i (t_j - \frac{s_j}{N}) k} e^{-2\pi i \frac{s_j k}{N}}. \quad (38)$$

We obtain the matrix decomposition

$$F_{\text{II}} = B \circ F_{\vec{s}}, \quad (39)$$

where $(F_{\vec{s}})_{j,k} = e^{-2\pi i s_j k/N}$, and $B_{jk} = e^{-2\pi i (t_j - s_j/N) k}$. Note that $(F_{\vec{s}})_{j,k}$ is the (k, s_j) -th entry of the DFT matrix, F . As before, the matrix B admits a rank- K approximation via a truncated bivariate Chebyshev approximation applied to each entry. The resulting rank- K approximation of B is then given by

$$B_K = \sum_{r=0}^{K-1} \underbrace{\left[\sum_{q=0}^{K-1} \alpha'_{qr} \left(\exp(-i\pi N(\vec{t} - \vec{s}/N)) \circ T_q(2N(\vec{t} - \vec{s}/N)) \right) \right]}_{\vec{u}_r} \underbrace{T_r\left(\frac{2\vec{\omega}^\top}{N} - \vec{1}^\top\right)}_{\begin{cases} 2\vec{v}_r^\top & r=0 \\ \vec{v}_r^\top & r \geq 1 \end{cases}}. \quad (40)$$

Here $\vec{s} = (s_0, s_1, \dots, s_{N-1})$ and $\vec{\omega} = (0, 1, \dots, N-1)$. The coefficient $\alpha'_{qr} \propto \alpha_{qr}$ in Equation (33) is defined with the choice $\gamma = \frac{1}{2}$. Note that $F_{\vec{s}} = F M_{\vec{s}}$, where

$$(M_{\vec{s}})_{ij} = \begin{cases} 1, & \text{if } i = s_j, \\ 0, & \text{otherwise,} \end{cases} \quad (41)$$

for $0 \leq i, j \leq N-1$. Consequently, F_{II} in the general case can then be approximated as

$$F_{\text{II}} = (B \circ F) \approx (B_K \circ F) = \sum_{r=0}^{K-1} D_{\vec{u}_r} F_{\vec{s}} D_{\vec{v}_r} = \sum_{r=0}^{K-1} D_{\vec{u}_r} F M_{\vec{s}} D_{\vec{v}_r}. \quad (42)$$

Once again, it suffices to choose $K = \mathcal{O}\left(\frac{\log(1/\epsilon'_{\text{trunc}})}{\log \log(1/\epsilon'_{\text{trunc}})}\right)$ to guarantee that $\|B - B_K\|_{\max} \leq \epsilon'_{\text{trunc}}$. The overall computational complexity of the algorithm remains as stated in Equation (36).

3.2. Reduction to Type-II NUDFT. Algorithms for Type-I and Type-III NUDFTs can now be derived from those of the Type-II NUDFT.

(I) **Type-I NUDFT.** The Type-I NUDFT can be efficiently implemented using the Type-II NUDFT. In particular, the entries of the matrix F_I satisfy

$$(F_I)_{jk} = e^{-2\pi i \frac{j}{N} \omega_k} = e^{-2\pi i \frac{\omega_k}{N} j} = (F_{II})_{kj}, \quad (43)$$

which shows that F_I is the transpose of F_{II} , where now $\frac{\omega_0}{N}, \dots, \frac{\omega_{N-1}}{N}$ assume the role of non-equispaced sample points in a Type-I NUDFT. Hence, F_I can be approximated as

$$F_I = F_{II}^T \approx \sum_{r=0}^{K-1} (D_{\vec{u}_r} F M_{\vec{s}} D_{\vec{v}_r})^T = \sum_{r=0}^{K-1} D_{\vec{v}_r} M_{\vec{s}}^T F^T D_{\vec{u}_r}. \quad (44)$$

Note that F^T can be efficiently computed using the inverse FFT. Therefore, the Type-I NUDFT may be realized via the Type-II NUDFT, inheriting the same computational complexity.

(III) **Type-III NUDFT.** The Type-III NUDFT can be also efficiently implemented using the Type-II NUDFT. It is shown in [14] the entries of the matrix F_{III} satisfy

$$(F_{III}) = A \circ B \circ (F M_{\vec{s}}) := A \circ B \circ (F_I)_{\vec{s}}, \quad (45)$$

where $A_{jk} = e^{-2\pi i (t_j - s_j/N) \omega_k}$, B is a matrix of rank at most 2 and $(F_I)_{\vec{s}}$ is obtained extracting the columns indexed by (s_0, \dots, s_{N-1}) from F_I . Therefore, the Type-III NUDFT may be realized via the Type-II NUDFT, inheriting the same computational complexity.

4. QUANTUM ALGORITHM FOR NON-UNIFORM DISCRETE FOURIER TRANSFORM

We now present a quantum algorithm for the Non-Uniform Quantum Fourier Transform (NUQFT) based on the low-rank factorization framework reviewed in Section 3. Throughout, we assume that $N = 2^n$ for some $n \geq 1$ and restrict attention to the Type-II NUQFT. The overall approach may be summarized as follows:

(1) **Construction of $U_{\vec{v}_r}$.** We first construct quantum circuits that encode the coefficient vectors \vec{v}_r , defined as follows:

$$(\vec{v}_r)_j = \begin{cases} 2^{-1} T_0(2j/N - 1), & r = 0, \\ T_r(2j/N - 1), & r \geq 1. \end{cases} \quad (46)$$

For each r , we construct a unitary operator $U_{\vec{v}_r}$ that encodes the entries of \vec{v}_r as amplitudes of a quantum state.

(2) **Construction of $U_{\vec{u}_r}$.** We next construct quantum circuits that encode the coefficient vectors \vec{u}_r , defined as follows:

$$(\vec{u}_r)_j = \sum_{q=0}^{K-1} \alpha'_{qr} e^{-i\pi N(t_j - s_j/N)} T_q(2N(t_j - s_j/N)). \quad (47)$$

For each r , we construct a unitary operator $U_{\vec{u}_r}$ that encodes the entries of \vec{u}_r as amplitudes of a quantum state.

(3) **Block-encoding Operators.** Using $U_{\vec{v}_r}$ and $U_{\vec{u}_r}$, we implement block encodings of the diagonal matrices $D_{\vec{v}_r}$ and $D_{\vec{u}_r}$. These are combined with a standard block encoding of the Fourier transform and the matrix $M_{\vec{s}}$ defined in Equation (41).

(4) **Assembly via LCU.** Finally, we employ the Linear Combination of Unitaries (LCU) algorithm to combine the block-encoded matrix products, thereby implementing a block encoding of the Type-II non-uniform discrete Fourier transform.

In what follows, we adopt the following convention. A quantum register refers to a system of qubits prepared in a superposition over computational basis states. Ancilla qubits are auxiliary qubits used to facilitate intermediate operations within a quantum circuit, whereas a computational

qubit denotes the qubit on which the final result of the computation is stored. We will explicitly specify any instance in which this convention is altered.

4.1. Construction of U_{v_r} . We first construct $U_{\vec{v}_r}$. The case $r = 0$ is particularly simple, since $(\vec{v}_0)_{j,j} = \frac{1}{2}$ because $T_0(x) \equiv 1$. We prepare a quantum register encoding j in uniform superposition, together with an ancilla qubit whose $|0\rangle$ amplitude represents the constant value $\frac{1}{2}$ for all j in the superposition. The corresponding quantum circuit, denoted $U_{\vec{v}_0}$, can therefore be implemented directly.

Proposition 7. *Let $n \in \mathbb{N}$. The unitary operator $U_{\vec{v}_0}$ can be implemented using $\mathcal{O}(n)$ Hadamard gates and $\mathcal{O}(1)$ single-qubit rotation gates.*

Proof. Prepare an n -qubit register in uniform superposition over all computational basis states using n Hadamard gates. Next, prepare a single computational qubit in the state $\frac{1}{2}|0\rangle + \frac{i\sqrt{3}}{2}|1\rangle$ using a single-qubit rotation of the form $e^{i\pi/3\sigma_X}$. This defines the unitary $U_{\vec{v}_0}$. The corresponding pseudocode is given in Algorithm 2. \square

Algorithm 2: Preparation of $U_{\vec{v}_0}$

```

Input: Integer  $n \geq 1$ 
Output: Quantum state with  $U_{\vec{v}_0}$  applied in superposition
Initialize  $(n+1)$  qubits  $|0\rangle|0\rangle^n$ 
for  $i \leftarrow 2$  to  $n+1$  do
     $\quad$  Apply Hadamard gate  $H$  to qubit  $i$  in  $|0\rangle^n$ 
    Apply single-qubit rotation  $e^{i\pi/3\sigma_X}$  to the computational qubit
return Quantum state  $U_{\vec{v}_0}|0\rangle|0\rangle^n = \frac{1}{\sqrt{2^n}} \sum_j \left( \frac{1}{2}|0\rangle + \frac{i\sqrt{3}}{2}|1\rangle \right) |j\rangle$ 

```

Lemma 8. *Let $k \in \mathbb{N}$ and let $x \in (0, 1)$ be stored in binary in a k -qubit computational register. There exists a quantum circuit U_{neg} acting on the k -qubit register such that $U_{\text{neg}}|x\rangle = |1-x\rangle$. Moreover, U_{neg} can be implemented using $\mathcal{O}(k)$ σ_X gates, $\mathcal{O}(k)$ CNOT gates, and $\mathcal{O}(k)$ Toffoli gates.*

Proof. Let $x = 0.x_1x_2\dots x_k$ be a k -bit fractional number expressed in binary, so that $x = \sum_{i=1}^k x_i 2^{-i}$. We define the bitwise complement of x as $\bar{x} = 0.\bar{x}_1\bar{x}_2\dots\bar{x}_k$, where $\bar{x}_i = 1 - x_i$ for each $i = 1, \dots, k$. Then

$$\bar{x} = \sum_{i=1}^k \bar{x}_i \cdot 2^{-i} = \sum_{i=1}^k (1 - x_i) 2^{-i} = \sum_{i=1}^k 2^{-i} - \sum_{i=1}^k x_i 2^{-i} = 1 - 2^{-k} - \sum_{i=1}^k x_i 2^{-i} = 1 - x - 2^{-k}. \quad (48)$$

\bar{x} can be computed by applying the σ_X gate to each of the k qubits. It remains to add 2^{-k} . This is a standard application of binary arithmetic and can be implemented by invoking the oracle U_{AM} using $\mathcal{O}(k)$ CNOT and Toffoli gates. The resulting quantum circuit is denoted by U_{neg} . \square

We now construct $U_{\vec{v}_r}$ for $r \geq 1$. In Proposition 9, a parameter $p \in \mathbb{N}$ is selected to facilitate the approximation of $\arccos(\cdot)$ on a quantum computer to arbitrary precision. This parameter is chosen freely at this stage, and will be fixed to a specific value later when required.

Proposition 9. *Let $p, r, n \in \mathbb{N}$. $U_{\vec{v}_r}$ can be implemented using $\mathcal{O}(n)$ Hadamard gates, $\mathcal{O}(n+p^2)$ CNOT gates, $\mathcal{O}(n)$ σ_X gates and $\mathcal{O}(p)$ single-qubit controlled rotation gates generated by σ_X . The corresponding quantum circuit has depth $\mathcal{O}(p \log p)$.*

Proof. Initialize two quantum registers of n qubits, p ancilla qubits, and one computational qubit, all initialized to $|0\rangle$. We index the first quantum register of n qubits from 0 to $n - 1$. Apply Hadamard gates to the first quantum register to construct the state $\frac{1}{\sqrt{2^n}} \sum_{j=0}^{2^n-1} |0\rangle |j\rangle |0\rangle^n |0\rangle^p$. Let

$$x_j := \frac{2j}{N} - 1 = \frac{\sum_{k=0}^{n-1} j_k 2^k}{2^{n-1}} - 1 = \sum_{k=0}^{n-1} j_k 2^{k-n+1} - 1 = \sum_{k=0}^{n-2} j_k 2^{k-(n-1)} + j_{n-1} - 1 \in [-1, 1]. \quad (49)$$

We first represent x_j in a fixed-point binary format. In what follows, we index the qubits in the second quantum register from 1 to n . The construction proceeds as follows:

- (1) For $k = 0$ to $n - 2$, apply a CNOT gate with the control on the k -th qubit of the first quantum register and the target on the m -th qubit of the second quantum register, where $m + k = n - 1$. This step ensures that the first $n - 1$ qubits in the second quantum register encode the fraction $\sum_{k=0}^{n-2} j_k 2^{k-n+1}$.
- (2) If $j_{n-1} = 1$, the construction is complete. If $j_{n-1} = 0$, then we must compute $\sum_{k=0}^{n-2} j_k 2^{k-n+1} - 1 \in [-1, 0)$. This is achieved by applying a controlled unitary operator, with the control on the last qubit of the first quantum register and the target on the second quantum register. The operator acts only if the control qubit is in the state $|0\rangle$. The sign is stored in the last qubit of the second quantum register, with $|1\rangle$ denoting a negative sign, while the first $n - 1$ qubits encode the absolute value

$$\left| \sum_{k=0}^{n-2} j_k 2^{k-(n-1)} - 1 \right| = 1 - \sum_{k=0}^{n-2} j_k 2^{k-(n-1)}. \quad (50)$$

This can be implemented using Lemma 8.

We now construct the entry $(\vec{v}_r)_j$ in superposition using the quantum signal processing (QSP) algorithm. We implement $e^{ir \arccos(x_j) \sigma_X}$. This requires computing $\theta_j = \arccos(x_j)$, which can be obtained by first computing $\arcsin(x_j)$ using the algorithm of Burge et al. [51] as in Section 2.3.1, and then applying $\arccos(x_j) = \pi/2 - \arcsin(x_j)$. Using the p ancilla qubits to store the approximation $\hat{\theta}_j = \widehat{\arccos}(x_j)$ ³, we have

$$|\hat{\theta}_j - \theta_j| \leq 2^{-p+1}. \quad (51)$$

We label this unitary operator U_{\arccos} , which can be implemented using $\mathcal{O}(p^2)$ CNOT gates and a circuit of depth $\mathcal{O}(p \log p)$. Note that we can write

$$\hat{\theta}_j = b_1^{(\theta_j)} 2^1 + b_0^{(\theta_j)} 2^0 + \sum_{k=-1}^{-(p-2)} b_k^{(\theta_j)} 2^k := \sum_{k=1}^{-(p-2)} b_k^{(\theta_j)} 2^k, \quad b_k^{(\theta_j)} \in \{0, 1\}, \quad (52)$$

since $\theta \in [0, \pi]$. We can implement $e^{ir\hat{\theta}_j \sigma_X} := R_X(-r\hat{\theta}_j)$ via the following formula:

$$R_X(-r\hat{\theta}_j) = R_X \left(-r \sum_{k=1}^{-(p-2)} b_k^{(\theta_j)} 2^k \right) = \prod_{k=1}^{-(p-2)} R_X(-r 2^k)^{b_k^{(\theta_j)}}. \quad (53)$$

If we adopt the convention of numbering the qubits in the p -qubit register from 1 down to $-(p-2)$, we have

$$R_X(-r\hat{\theta}_j) = \prod_{k=1}^{-(p-2)} \left(|0\rangle\langle 0|_k \otimes I + |1\rangle\langle 1|_k \otimes R_X(-r 2^k) \right), \quad (54)$$

³The p -bit binary representation of $\pi/2$ can be computed classically and used to obtain a p -bit approximation of $\pi/2 - \arcsin(x_j)$ in the p -qubit register containing $\hat{\theta}_j = \widehat{\arcsin}(x_j)$. Since this operation does not change the overall circuit complexity, we assume that it is incorporated within the quantum circuit, U_{\arccos} .

where each of the control qubits is one of the p ancilla qubits. This step requires $\mathcal{O}(p)$ applications of single-qubit controlled rotation gates generated by σ_X . Using [52, Equation (45)], which provides the explicit expression for $e^{ir \arccos(x) \sigma_X}$, the resulting quantum state is given by

$$U_{\vec{v}_r} |0\rangle |0\rangle^{2n} |0\rangle^p = \frac{1}{\sqrt{2^n}} \sum_{j=0}^{2^n-1} \left(T_r(x_j) |0\rangle + i\sqrt{1-x_j^2} S_{r-1}(x_j) |1\rangle \right) |j\rangle |x_j\rangle^n |\widehat{\arccos}(x_j)\rangle^p. \quad (55)$$

See Algorithm 3 and Figure 3 for the corresponding pseudocode and quantum circuit. \square

Algorithm 3: Construction of $U_{\vec{v}_r}$ for $r \geq 1$

Input: $p, n, r \in \mathbb{N}$ and U_{neg} from Lemma 8

Output: Quantum state with $U_{\vec{v}_r}$ applied in superposition

Initialize $1 + 2n + p$ qubits to $|0\rangle$

Apply Hadamard gates to first register of n qubits

for $k \leftarrow 0$ **to** $n - 2$ **do**

\sqcup Apply CNOT with control k in 1st register and target $m = n - k - 1$ in 2nd register

 Apply C-U_{neg} with control last qubit of 1st register and target first $n - 1$ qubits on 2nd register

 Apply CNOT with control last qubit of 1st register and target last qubit on 2nd register

 Compute (an approximation to) $\theta_j = \arccos(x_j)$ using U_{\arccos} on p -qubit ancilla

for $k \leftarrow 1$ down to $-(p - 2)$ **do**

\sqcup **if** $b_k^{(\theta_j)} = 1$ in θ_j register **then**

\sqcup Apply controlled rotation $e^{ir2^k \sigma_X}$ with control on ancilla qubit k

return Quantum state $U_{\vec{v}_r} |0\rangle |0\rangle^{2n} |0\rangle^p$

The second quantum register of n qubits, together with the p ancilla qubits, can be uncomputed, yielding a unitary $U'_{\vec{v}_r}$ such that

$$U'_{\vec{v}_r} |0\rangle |0\rangle^{2n} |0\rangle^p = \frac{1}{\sqrt{2^n}} \sum_{j=0}^{2^n-1} \left(T_r(x_j) |0\rangle + i\sqrt{1-x_j^2} S_{r-1}(x_j) |1\rangle \right) |j\rangle |0\rangle^n |0\rangle^p. \quad (56)$$

This step does not alter the computational complexity of the quantum circuit. For notational simplicity, we continue to denote $U'_{\vec{v}_r}$ by $U_{\vec{v}_r}$.

4.2. Construction of U_{u_r} . We now construct $U_{\vec{u}_r}$. The expression for $(\vec{u}_r)_j$ is determined by $\vec{t} \in [0, 1]^{2^n}$. Since \vec{t} is arbitrary, we assume access to the following oracle as part of the algorithm.

Assumption 10. For $m \geq n$, we assume access to the oracle $O_{\vec{t}}^{(m)}$ such that

$$O_{\vec{t}}^{(m)} : |i\rangle |0\rangle^m \mapsto |i\rangle |t_i^{(m)}\rangle^m = \bigotimes_{j=1}^m |i\rangle |t_i^{(j)}\rangle, \quad (57)$$

where $t_i^{(m)} = \sum_{j=1}^m t_i^{(j)} 2^{-j} = 0.t_i^{(1)} \cdots t_i^{(m)}$ is the m -bit binary representation of t_i . The parameter m is left arbitrary for now and will be fixed to a specific value as required.

The first step is to compute $\vec{s} = (s_0, s_1, \dots, s_{2^n-1})$, as defined in Equation (37). The vector \vec{s} can be computed as

$$s_i = \begin{cases} \text{round}(Nt_i) & \text{if } \text{round}(Nt_i) < N \\ 0 & \text{if } \text{round}(Nt_i) = N, \end{cases} \quad (58)$$

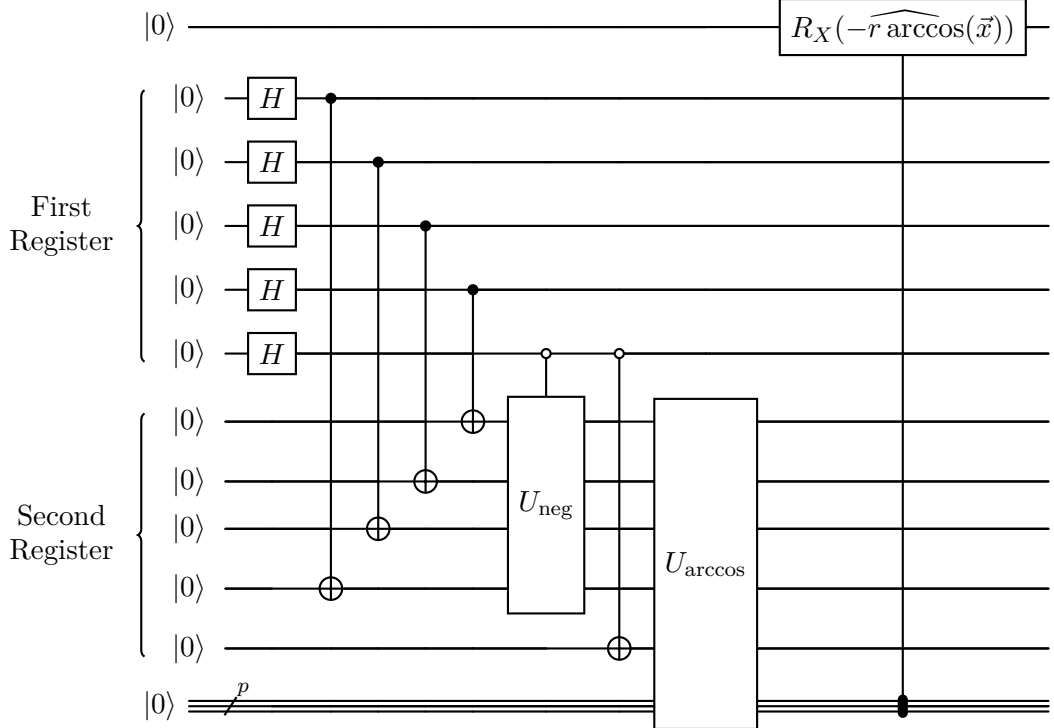


FIGURE 3. Quantum circuit implementing $U_{\vec{v}_r}$ for $r \geq 1$ in the special case $n = 5$.

where $N = 2^n$ and $\text{round}(\cdot)$ denotes rounding to the nearest integer. In fact, we now explicitly construct a quantum circuit that implements the oracle

$$O_{\vec{s}}^{(m)} : |i\rangle |0\rangle^m \mapsto |i\rangle |s_i^{(m)}\rangle^m = \bigotimes_{j=1}^m |i\rangle |s_i^{(j)}\rangle, \quad (59)$$

where $s_i^{(m)}$ is the m -bit representation of s_i/N . We first claim that the operation $N\vec{t}$ can be implemented efficiently.

Lemma 11. *Let $n \in \mathbb{N}, m \geq n$ and $\vec{t} \in [0, 1]^{2^n}$. $N\vec{t}$ can be computed using $\mathcal{O}(1)$ queries to $O_{\vec{t}}^{(m)}$ and $\mathcal{O}(n)$ Hadamard gates on an $\mathcal{O}(n+m)$ qubit circuit.*

Proof. Initialize an $(n+m)$ -qubit quantum register in $|0\rangle$. Apply Hadamard gates to the first n qubits to prepare the uniform index superposition $\frac{1}{\sqrt{2^n}} \sum_{i=0}^{2^n-1} |i\rangle |0\rangle^m$. Querying $O_{\vec{t}}^{(m)}$ yields

$$O_{\vec{t}}^{(m)} |0\rangle^{n+m} = \frac{1}{\sqrt{2^n}} \sum_{i=0}^{2^n-1} \bigotimes_{j=1}^m |i\rangle |t_i^{(j)}\rangle. \quad (60)$$

Multiplication by N yields $Nt_i^{(m)} = t_i^{(1)} \dots t_i^{(n)} \cdot t_i^{(n+1)} \dots t_i^{(m)}$, where the first n bits correspond to $\lfloor Nt_i \rfloor$, and the remaining $m - n$ bits correspond to the fractional part. No additional quantum gates are required. \square

The next step is to round each Nt_i to the nearest integer, a nontrivial operation only when $|t_i^{(n+1)}\rangle = 1$. This rounding can be implemented as a controlled unitary, denoted U_{round} . In this setting, rounding the binary string $t_i^{(1)} \dots t_i^{(n)}$ amounts to computing the binary sum $t_i^{(1)} \dots t_i^{(n)} \oplus 1$. Equivalently, this corresponds to the map $|x\rangle \mapsto |x \oplus y\rangle$, where $|x\rangle = |t_i^{(1)} \dots t_i^{(n)}\rangle$ and $|y\rangle = |t_i^{(n+1)}\rangle$. This operation can be realized using the oracle U_{AM} .

Proposition 12. Let $n \in \mathbb{N}$ and $m \geq n$. The oracle $O_{\vec{s}}^{(m)}$ can be implemented using a $\mathcal{O}(n + m)$ -qubit quantum circuit, $\mathcal{O}(1)$ queries to the oracle $O_{\vec{t}}^{(m)}$, $\mathcal{O}(n)$ Hadamard gates and $\mathcal{O}(m)$ Toffoli, CNOT and σ_X gates.

Proof. This follows directly from Lemma 11 together with the use of U_{AM} , noting that the m -bit representation of s_i/N is stored in the m -qubit register upon application of circuit in Figure 4. \square

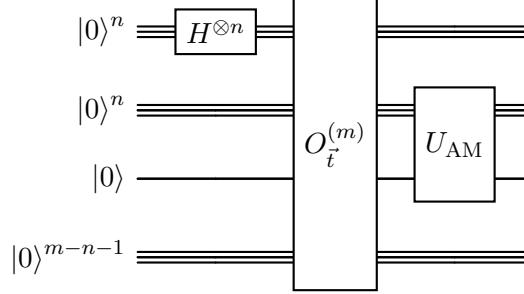


FIGURE 4. Quantum circuit implementing $O_{\vec{s}}^{(m)}$.

Having constructed the oracle $O_{\vec{s}}^{(m)}$, the next step is to construct $U_{\vec{u}_r}$ for $r \geq 0$, which implements $(\vec{u}_r)_j$. We first establish a lemma analogous to Lemma 8, which enables the computation of $x - y$ for $x, y \in [0, 1)$ using the quantum circuit U_{subtract} .

Remark 13. In what follows, when we say that a quantum register is “multiplied by 2^k ” for some $k \geq 1$, we mean a reinterpretation of the same qubit register under a fixed-point encoding in which the binary point is shifted k positions to the right. No quantum gates are applied; this operation is purely a change in the numerical interpretation of the register contents. Conversely, “division by 2^k ” corresponds to shifting the binary point k positions to the left.

Lemma 14. Let $m \in \mathbb{N}$ and let $x, y \in [0, 1)$ be stored in k -qubit registers. There exists a unitary operator U_{subtract} that computes the signed difference $x - y \in (-1, 1)$ using $\mathcal{O}(k)$ CNOT, Toffoli, and σ_X gates.

Proof. Let $x = 0.x_1x_2\dots x_k$ and $y = 0.y_1y_2\dots y_k$ be the k -bit fractional binary representations of x and y , so that $x = \sum_{i=1}^k x_i 2^{-i}$ and $y = \sum_{i=1}^k y_i 2^{-i}$. Multiply x and y by 2^k to obtain integers

$$X = \sum_{i=1}^k x_i 2^{k-i} = x \cdot 2^k, \quad Y = \sum_{i=1}^k y_i 2^{k-i} = y \cdot 2^k. \quad (61)$$

Note that $X, Y \in \{0, 1, \dots, 2^k - 1\}$. Embed X and Y into $(k+1)$ -qubit registers by adding a leading sign bit set to 0, thereby interpreting them as signed integers. We have

$$X = 0 \cdot 2^k + \sum_{i=1}^k x_i 2^{k-i}, \quad Y = 0 \cdot 2^k + \sum_{i=1}^k y_i 2^{k-i}. \quad (62)$$

Compute the bitwise complement of Y :

$$\bar{Y} = 1 \cdot 2^k + \sum_{i=1}^k \bar{y}_i 2^{k-i} = 1 \cdot 2^k + \sum_{i=1}^k (1 - y_i) 2^{k-i} = 1 \cdot 2^k + \sum_{i=1}^k 2^{k-i} - \sum_{i=1}^k y_i 2^{k-i} = 2^{k+1} - Y - 1. \quad (63)$$

\bar{Y} by applying a σ_X gate to each of the $k+1$ qubits representing Y . Add 1 to obtain $-Y := \bar{Y} + 1 = 2^{k+1} - Y$, ignoring any overflow. It is well known in binary arithmetic that $\bar{Y} + 1$ corresponds to the negative of Y , provided that the signed bit, which is the $(k+1)$ -st qubit, is subtracted from

the binary number represented by the first k qubits.⁴ This justifies the notation $-Y$ for $\bar{Y} + 1$. Next, use U_{AM} to compute X and $-Y$. This produces the signed integer $Z := X + (-Y) = X - Y$. Finally, we interpret Z as a fixed-point number by dividing by 2^k , thereby obtaining the signed real value $\frac{Z}{2^k} = x - y \in (-1, 1)$. Since $x, y \in [0, 1]$, no overflow occurs beyond the representable range. The overall circuit uses $\mathcal{O}(k)$ CNOT, Toffoli, and σ_X gates. \square

Algorithm 4: Computation of $x - y$ using signed fixed-point arithmetic (U_{subtract})

Input: k -qubit registers $|x\rangle = |x_1 \cdots x_k\rangle$ and $|y\rangle = |y_1 \cdots y_k\rangle$ encoding $x, y \in [0, 1]$

Output: $(k + 1)$ -qubit register encoding the signed fixed-point value $x - y$

Scale $|x\rangle$ and $|y\rangle$ by 2^k to obtain integer registers $|X\rangle$ and $|Y\rangle$

Append a leading qubit $|0\rangle$ to each register to form signed $(k + 1)$ -qubit registers

for $i \leftarrow 1$ **to** $k + 1$ **do**

\sqcup Apply σ_X to qubit i of $|Y\rangle$

 Add 1 to $|Y\rangle$ to obtain the two's-complement encoding of $-Y$

 Compute $|X - Y\rangle$ using U_{AM}

 Interpret the result as a signed fixed-point number by dividing by 2^k

return Computational register representing $|x - y\rangle$

We now construct $U_{\vec{u}_r}$ for $r \geq 0$. The approach applies the previous constructions to compute $\vec{t} - \vec{s}/N$, followed by the implementation of $T_q(2N(\vec{t} - \vec{s}/N))$ via quantum signal processing (QSP). Complex exponential factors are realized as rotations generated by σ_Z , and the weighted Chebyshev terms are summed using the linear combination of unitaries (LCU) method. As in Proposition 9, a parameter $p \in \mathbb{N}$ is introduced to approximate $\arccos(\cdot)$ with arbitrary precision and will later be fixed as needed. We also assume access to a specific state-preparation oracle.

Assumption 15. We assume access to a state-preparation oracle

$$\text{PREP}_r |0\rangle = \frac{1}{\sqrt{\|\vec{\alpha}'_r\|_1}} \sum_{q=0}^{K-1} \sqrt{\alpha'_{qr}} |q\rangle, \quad (64)$$

where α'_{qr} are defined in Equation (33) and Equation (34) with $\gamma = 1/2$.

Proposition 16. Let $m, p, K \in \mathbb{N}$ and $r \in \mathbb{N} \cup \{0\}$. $U_{\vec{u}_r}$ can be implemented using $\mathcal{O}(m + n + p + \log K)$ qubits, $\mathcal{O}(1)$ queries to $O_{\vec{t}}^{(m)}$, $\mathcal{O}(n)$ Hadamard gates, $\mathcal{O}(m + p^2)$ CNOT gates, $\mathcal{O}(m)$ Toffoli gates, $\mathcal{O}(m)$ σ_X gates, and $\mathcal{O}(p + m)$ single-qubit controlled rotation gates. The corresponding quantum circuit has depth $\mathcal{O}(m + p \log p + \log K)$.

Proof. Consider a $(1 + n + 2m + p)$ -qubit system, with all qubits initialized to $|0\rangle$. First, apply Hadamard gates to the quantum register of n qubits, and then apply the oracles $O_{\vec{t}}^{(m)}$ and $O_{\vec{s}}^{(m)}$ on the two m -qubit ancilla registers to construct the state

$$\frac{1}{\sqrt{2^n}} \sum_{i=0}^{2^n-1} |0\rangle |i\rangle |t_i^{(m)}\rangle^m |s_i^{(m)}\rangle^m / N^m |0\rangle^p. \quad (65)$$

Invoking Lemma 14, we compute $\vec{t} - \vec{s}/N$ in superposition within the quantum register containing \vec{s}/N .⁵ We then compute an approximation of $\arccos(2N(\vec{t} - \vec{s}/N))$. The multiplication by $2N$ is implemented reversibly as a constant-factor scaling on the fixed-point representation of $\vec{t} - \vec{s}/N$.

⁴The expression $-Y := \bar{Y} + 1$ is called “two's complement” in binary arithmetic.

⁵A single ancilla qubit can be appended to encode the sign of $t_j - s_j/N$ without affecting the overall circuit complexity. This ancilla qubit is used in Lemma 14, and the stored sign is subsequently employed to approximate \arccos via the algorithm of [51].

Algorithm 5: Implementation of $U_{\vec{u}_r}$

Input: Integers $n, m, p \geq 1$, system size $n + 2m + p + 1$ qubits
Output: Operator $U_{\vec{u}_r} = \sum_{q=0}^{K-1} \alpha'_{qr} U_{qr}$ applied in superposition

Initialize all $n + 2m + p + 1$ qubits to $|0\rangle$
 Apply Hadamard gates $H^{\otimes n}$ to the n -qubit register
 Apply oracles $O_{\vec{t}}^{(m)}$ and $O_{\vec{s}}^{(m)}$ to the two m -qubit registers
 Compute $\vec{t} - \vec{s}/N$ in the \vec{t} -register using U_{subtract} (see Algorithm 4)
 Apply U_{arccos} to approximate $\arccos(\vec{t} - \vec{s}/N)$ in the p -qubit register
 Apply controlled rotation $R_X(-q \arccos(2N(\vec{t} - \vec{s}/N)))$ to realize $T_q(x)$
 Apply controlled rotation $R_Z(\pi N(\vec{t} - \vec{s}/N))$ to realize $e^{-i\pi N(\vec{t} - \vec{s}/N)}$
 Append $\mathcal{O}(\log K)$ ancilla qubits
 Denote the resulting unitary as U_{qr}
 Use LCU method to implement $U_{\vec{u}_r} = \sum_{q=0}^{K-1} \alpha'_{qr} U_{qr}$ via U_{LCU}
return $U_{\vec{u}_r} |0\rangle^{(n+2m+p+1+\mathcal{O}(\log K))}$

Since $2N$ is a power of two, this operation reduces to a bit shift and therefore does not affect the overall complexity of the quantum circuit. By invoking U_{arccos} as in Proposition 9, we obtain an approximation of $\arccos(2N(\vec{t} - \vec{s}/N))$ in superposition within the p -qubit register. We denote the quantum circuit implementing this scaling step followed by U_{arccos} by U'_{arccos} . As in Proposition 9, we implement a controlled rotation $R_X(-q \arccos(2N(\vec{t} - \vec{s}/N)))$ to realize the Chebyshev polynomial $T_q(x)$. Similarly, we implement a controlled rotation $R_Z(\pi N(\vec{t} - \vec{s}/N))$ to realize the phase factor $e^{-i\pi N(\vec{t} - \vec{s}/N)}$. Denote the unitary operator constructed above by U_{qr} . Finally, using the state-preparation oracle in Equation (64), we apply the LCU algorithm to implement the desired expression via the operator $U_{\vec{u}_r} = \sum_{q=0}^{K-1} \alpha'_{qr} U_{qr}$. We need to append an $\mathcal{O}(\log K)$ ancilla qubits to invoke the LCU algorithm. The complexity estimates follow from previous complexity estimates and the observation that a $\mathcal{O}(\log K)$ -qubit controlled gate acting can be implemented via a quantum circuit using only CNOT gates and single-qubit gates such that the circuit has depth $\mathcal{O}(\log K)$ [55]. If $y_i^{(m)} = t_i^{(m)} - s_i^{(m)}/N$, the resulting quantum state $U_{\vec{u}_r} |0\rangle^{(n+2m+p+1+\mathcal{O}(\log K))}$ is given by

$$\frac{1}{\sqrt{2^n}} \sum_{i=0}^{2^n-1} \left(\frac{1}{\|\vec{\alpha}'_r\|_1} \left(\sum_{q=0}^{K-1} \alpha'_{qr} U_{qr} |0\rangle \right) |0\rangle^{\mathcal{O}(\log K)} + |\perp\rangle \right) |i\rangle |t_i^{(m)}\rangle^m |y_i^{(m)}\rangle^m |\widehat{\arccos}(y_i^{(m)})\rangle^p, \quad (66)$$

where $|\perp\rangle$ is a state that is orthogonal to $(\sum_{q=0}^{K-1} \alpha'_{qr} U_{qr} |0\rangle) |0\rangle^{\mathcal{O}(\log K)}$. See Figure 5 for the corresponding quantum circuit and Algorithm 5 for the corresponding pseudocode. \square

Once again, the ancilla qubits can be uncomputed, yielding a unitary $U'_{\vec{u}_r}$ such that the output quantum state is

$$\frac{1}{\sqrt{2^n}} \sum_{i=0}^{2^n-1} \left(\frac{1}{\|\vec{\alpha}'_r\|_1} \left(\sum_{q=0}^{K-1} \alpha'_{qr} U_{qr} |0\rangle \right) |0\rangle^{\mathcal{O}(\log K)} + |\perp\rangle \right) |i\rangle |0\rangle^{2m} |0\rangle^p. \quad (67)$$

This step does not change the computational complexity of the quantum circuit. For notational simplicity, we continue to denote $U'_{\vec{v}_r}$ by $U_{\vec{v}_r}$. Note that, in Figure 5, we have departed from the usual convention of placing the ancilla qubits $|0\rangle^{\mathcal{O}(\log K)}$ below the n -qubit register. This deviation was necessary to avoid awkward placement of the U_{LCU} gate in the circuit diagram.

4.3. Block Encoding Operators. We now use $U_{\vec{u}_r}$ and $U_{\vec{v}_r}$ within a block-encoding framework to implement the diagonal matrices $D_{\vec{u}_r}$ and $D_{\vec{v}_r}$. We assume that the ancilla qubits used to implement $U_{\vec{v}_r}$ and $U_{\vec{u}_r}$ have been uncomputed, as discussed above. These qubits will not be

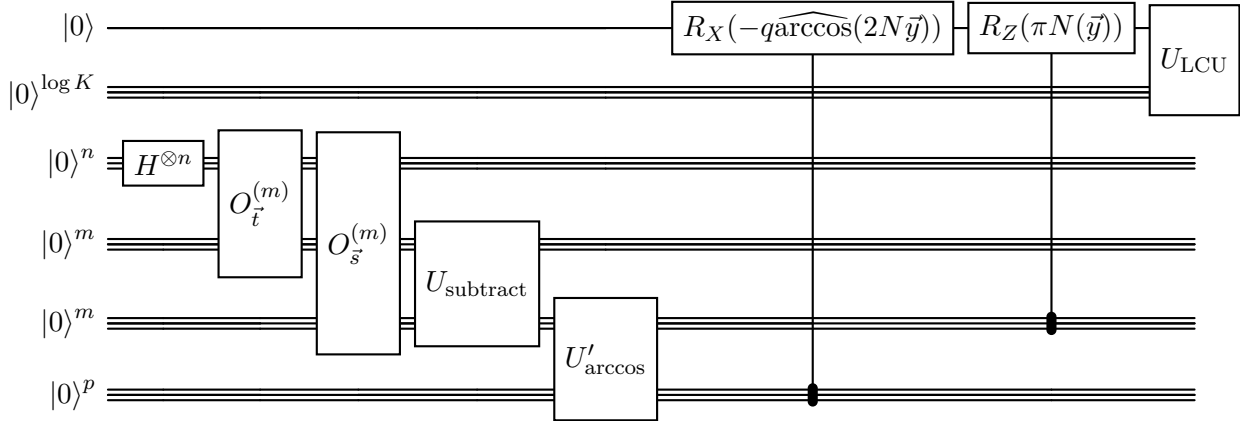


FIGURE 5. Quantum circuit implementing the operator $U_{\vec{u}_r} = \sum_{q=0}^{K-1} \alpha'_{qr} U_{qr}$. We have abbreviated $\vec{t} - \vec{s}/N$ by \vec{y} .

referenced in any equations or quantum circuits below; however, their usage is accounted for in the overall complexity analysis of the algorithm in Theorem 21. Recall that $U_{\vec{v}_r}$ acts on $|j\rangle|0\rangle$ as

$$U_{\vec{v}_r}|j\rangle|0\rangle = |j\rangle(v_r(j)|0\rangle + \sqrt{1 - v_r(j)^2}|1\rangle). \quad (68)$$

The top-left block of $U_{\vec{v}_r}$ corresponds exactly to the desired diagonal matrix:

$$(\langle 0| \otimes I)U_{\vec{v}_r}(|0\rangle \otimes I) = D_{\vec{v}_r}. \quad (69)$$

This yields a $(1, 1, 0)$ block encoding of $D_{\vec{v}_r}$.

Example 17. Let $N = 4$, so that $D_{\vec{v}_r} = \text{diag}(v_r(0), v_r(1), v_r(2), v_r(3))$. We abbreviate $i\sqrt{1 - v_r(0)^2}$ as $v'_r(0)$. After uncomputing and ignoring any auxiliary registers, the matrix representation of $U_{\vec{v}_r}$ block encodes $D_{\vec{v}_r}$ as follows:

$$U_{\vec{v}_r} = \begin{pmatrix} v_r(0) & & & & * & & \\ & v_r(1) & & & * & & \\ & & v_r(2) & & & * & \\ & & & v_r(3) & & & * \\ \hline v'_r(0) & & & & * & & \\ & v'_r(1) & & & * & & \\ & & v'_r(2) & & & * & \\ & & & v'_r(3) & & & * \end{pmatrix} \quad (70)$$

We have adopted the basis convention $\{|000\rangle, |010\rangle, |100\rangle, |110\rangle, |001\rangle, |011\rangle, |101\rangle, |111\rangle\}$ in the matrix representation of $U_{\vec{v}_r}$ above, where the first qubit corresponds to the computational qubit. Projecting onto the computational state $|0\rangle$ extracts the top-left submatrix:

$$(\langle 0| \otimes I_4)U_{\vec{v}_r}(|0\rangle \otimes I_4) = \begin{pmatrix} v_r(0) & & & \\ & v_r(1) & & \\ & & v_r(2) & \\ & & & v_r(3) \end{pmatrix} = D_{\vec{v}_r}. \quad (71)$$

A similar argument yields a block encoding of $D_{\vec{u}_r}$. The only difference is that $D_{\vec{u}_r}/\|\vec{a}'_r\|_1$ is block encoded, since \vec{u}_r is implemented via the LCU method. Consequently, we obtain a $(\|\vec{a}'_r\|_1, 1, 0)$ block encoding of $D_{\vec{u}_r}$. Furthermore, recall that $F_{\vec{s}} = FM_{\vec{s}}$, where $M_{\vec{s}}$ is defined in Equation (41). Since F is unitary, a block encoding of F is immediate. Since $M_{\vec{s}}$ is a binary (0–1) matrix, we can apply Lemma 4 to obtain a block encoding of $M_{\vec{s}}$. Observe that $M_{\vec{s}}$ is a 1-column-sparse matrix

and that the oracle $O_{\vec{s}}^{(m)}$ effectively realizes the column-access oracle O_c . In this setting, it suffices to choose $m = n$. We further note that the row-access oracle O_r corresponds to access to the inverse mapping of $\vec{t} \mapsto \vec{s}$. For generic \vec{t} and \vec{s} , constructing O_r from $O_{\vec{t}}$ and $O_{\vec{s}}$ may require additional pre-processing or data-structure assumptions; accordingly, we treat O_r as an independent primitive.

Assumption 18. We assume black-box access to the row-access oracle O_r required by Lemma 4.

The oracle O_A can be implemented efficiently. Specifically, we construct O_A by appending an additional n -qubit register and applying $O_{\vec{s}}^{(n)}$ to obtain

$$|0\rangle^n |i\rangle |j\rangle |0\rangle \mapsto |s_j\rangle |i\rangle |j\rangle |0\rangle. \quad (72)$$

Noting that $A_{i,j} = \langle s_j | i \rangle$, we compute the inner product of the n -qubit registers $|s_j\rangle$ and $|i\rangle$, which are computational basis states, and store the resulting binary outcome in the last qubit, thereby encoding $A_{i,j}$. More formally, the entry $A_{i,j}$ is computed as follows.

Lemma 19. *Let $|i\rangle$ and $|s_j\rangle$ be n -qubit computational basis states, and define $A_{i,j} = \langle s_j | i \rangle \in \{0, 1\}$. Then there exists a unitary $U_{i,j}$ acting on an $2n + 1$ -qubit register such that*

$$U_{i,j}(|i\rangle |s_j\rangle |0\rangle) = |i\rangle |s_j\rangle |A_{i,j}\rangle.$$

Moreover, $U_{i,j}$ can be implemented using $\mathcal{O}(n)$ CNOT gates, $\mathcal{O}(n)$ σ_X gates, $\mathcal{O}(n)$ Toffoli gates and possibly $\mathcal{O}(n)$ ancilla qubits.

Proof. For $r = 1, \dots, n$, apply a CNOT gate with the r -th qubit of $|i\rangle$ as the control and the r -th qubit of $|s_j\rangle$ as the target. After this operation, the r -th qubit of $|s_j\rangle$ stores $i_r \oplus s_{j,r}$. Next, apply a σ_X gate to each qubit of $|s_j\rangle$ to obtain i_r XNOR $s_{j,r}$. Each qubit of $|s_j\rangle$ then stores 1 if $i_r = s_{j,r}$ and 0 otherwise. Finally, apply a C^n -AND gate with the n qubits of $|s_j\rangle$ as controls and the last qubit as the target. This sets the last qubit to 1 if and only if all transformed qubits of $|s_j\rangle$ are equal to 1. Hence, the last qubit correctly encodes $A_{i,j}$. The procedure uses $\mathcal{O}(n)$ CNOT gates, $\mathcal{O}(n)$ σ_X gates, and a single C^n -AND gate, which can be implemented using $\mathcal{O}(n)$ Toffoli gates and, if necessary, $\mathcal{O}(n)$ ancilla qubits. \square

Consider the vector

$$\vec{c}_s = (c_0^{s_0}, c_1^{s_1}, \dots, c_{2^n-1}^{s_{2^n-1}}) \quad (73)$$

where $c_i^{s_i}$ denotes the number of occurrences of s_i in \vec{s} . Noting that $M_{\vec{s}}$ is a 1-column sparse matrix and a $\|\vec{c}_s\|_\infty$ -row sparse matrix, we can construct a $\mathcal{O}(\sqrt{\|\vec{c}_s\|_\infty}, n + 3, 0)$ block-encoding of $M_{\vec{s}}$ by invoking Lemma 4.

Remark 20. The computational cost of the oracle for $M_{\vec{s}}$ discussed above is evaluated under the assumption that $m = n$. In what follows, m is treated as a free parameter with $m \geq n$. Under this assumption, the computational complexity of implementing the block encoding described in Lemma 19 does not affect the overall computational complexity of the algorithm derived in Theorem 21. Accordingly, it is omitted from the subsequent complexity analysis.

4.4. Assembly via LCU. The final step is to implement $\sum_{r=0}^{K-1} D_{\vec{u}_r} F_{\vec{s}} D_{\vec{v}_r}$ via a quantum circuit. This is achieved by combining the block encodings constructed above with the LCU algorithm. In Theorem 21, we present this procedure and derive the corresponding non-asymptotic complexity of the algorithm.

Theorem 21. *Let $n, m, p, K \in \mathbb{N}$ with $m \geq n$. There exists a quantum circuit, V_{II} , implementing a block encoding of $\sum_{r=0}^{K-1} D_{\vec{u}_r} F M_{\vec{s}} D_{\vec{v}_r}$ with normalization factor*

$$\alpha := K \sqrt{\|\vec{c}_s\|_\infty} \sum_{r=0}^{K-1} \|\vec{a}'_r\|_1. \quad (74)$$

and $\mathcal{O}(n + \log K)$ ancilla qubits. In other words, we have

$$(\langle 0 |^{\mathcal{O}(n + \log K)} \otimes I_{2^n}) V_{\text{II}} (|0\rangle^{\mathcal{O}(n + \log K)} \otimes I_{2^n}) = \frac{1}{\alpha} \sum_{r=0}^{K-1} D_{\vec{u}_r} F M_{\vec{s}} D_{\vec{v}_r}. \quad (75)$$

The circuit uses $\mathcal{O}(m + n + p + \log K)$ qubits, $\mathcal{O}(n + \log K)$ Hadamard gates, $\mathcal{O}(m + p^2)$ CNOT gates, $\mathcal{O}(m)$ Toffoli gates, $\mathcal{O}(m)$ σ_X gates, and $\mathcal{O}(p + m + n^2)$ single-qubit controlled rotation gates. The circuit depth is $\mathcal{O}(m + p \log p + \log K)$.

Proof. Fix $r \in \{0, \dots, K-1\}$. Prepare two single-qubit ancilla registers a_r and b_r together with an n -qubit system register. Observe that $I_{a_r} \otimes I_{b_r} \otimes U_{\text{QFT}}$ is a $(1, 2, 0)$ block encoding of U_{QFT} . By repeated application of Lemma 3, the unitary

$$U_r := (I_{b_r} \otimes U_{\vec{u}_r})(I_{a_r} \otimes I_{b_r} \otimes U_{\text{QFT}})(I_{a_r} \otimes U_{\vec{v}_r}) \quad (76)$$

is a $(\|\vec{a}'_r\|_1, 2, 0)$ block encoding of $D_{\vec{u}_r} F D_{\vec{v}_r}$. Using the construction described above for $M_{\vec{s}}$ and again invoking Lemma 3, we obtain a

$$(\|\vec{a}'_r\|_1 \sqrt{\|\vec{c}_s\|_\infty}, n+5, 0) \quad (77)$$

block encoding of $D_{\vec{u}_r} F M_{\vec{s}} D_{\vec{v}_r}$, which we continue to denote by U_r . To implement the sum $\sum_{r=0}^{K-1} D_{\vec{u}_r} F M_{\vec{s}} D_{\vec{v}_r}$, we apply the LCU algorithm. Introduce $\mathcal{O}(\log K)$ ancilla qubits and define the select unitary

$$\text{SEL} = \sum_{r=0}^{K-1} U_r \otimes |r\rangle\langle r|. \quad (78)$$

To implement the linear combination of unitaries (LCU), we assume access to a separate state-preparation oracle $\text{PREP} := H^{\otimes \mathcal{O}(\log K)}$. Conjugating SEL with PREP yields the standard LCU unitary. The resulting construction is therefore a

$$\left(\sum_{r=0}^{K-1} K \sqrt{\|\vec{c}_s\|_\infty} \|\vec{a}'_r\|_1, n+5+\log K, 0 \right) \quad (79)$$

block encoding of $\sum_{r=0}^{K-1} D_{\vec{u}_r} F M_{\vec{s}} D_{\vec{v}_r}$ [33, Lemma 52]. The stated gate counts, qubit complexity, and circuit depth follow from the previous complexity estimates, taking into account the costs of implementing each U_r as well as the overhead introduced by the LCU construction. \square

Note that the $\mathcal{O}(n^2)$ term in the expression $\mathcal{O}(p+n^2)$ in Theorem 21 arises from the requirement to apply $\mathcal{O}(n^2)$ controlled-rotation gates in the standard quantum circuit implementation of the Quantum Fourier Transform. We therefore observe that this quadratic dependence constitutes the dominant contribution to the overall gate-complexity estimates.

5. ERROR ANALYSIS

We now present an error analysis of the quantum algorithm implementing the Type-II NUDFT.

5.1. Error Sources. We first identify the sources of error arising in the quantum implementation of the algorithm.

- (1) **Truncation Error.** Antolín and Townsend [14] approximate the NUDFT matrix by a rank- K matrix from a Chebyshev expansion. To achieve $\|\cdot\|_{\max} \leq \epsilon_{\text{trunc}}$, choose $K = \mathcal{O}\left(\frac{\log(1/\epsilon'_{\text{trunc}})}{\log \log(1/\epsilon'_{\text{trunc}})}\right)$, for some $\epsilon'_{\text{trunc}} > 0$.
- (2) **Finite-Precision Oracle Error.** The sampling points t_j and s_j are given with m -bit precision, introducing errors in $t_j - s_j/N$ that propagate to the complex exponentials and Chebyshev evaluations.
- (3) **Arccosine Evaluation Error.** QSP implementation requires rotations by $\arccos(x)$. Computing $\arccos(x)$ to p -bit precision incurs error $\mathcal{O}(2^{-p})$.

(4) **Block-Encoding Error.** These errors accumulate in the block encoding of the constructed operators, reducing the overall accuracy of the resulting unitaries.

5.2. Error Bounds. We now bound the total error of the quantum algorithm and specify the parameters (K, m, p) so that the total error remains below the prescribed tolerance ϵ . Let \tilde{V}_{II} denote the approximately constructed version of the quantum circuit introduced in Theorem 21. Moreover, recall that we have approximated $F_{\text{II}} = A \circ (FM_{\vec{s}})$ on a quantum computer by implementing

$$\tilde{F}_{\text{II}} := A_K \circ (FM_{\vec{s}}) = \sum_{r=0}^{K-1} D_{\vec{u}_r} FM_{\vec{s}} D_{\vec{v}_r}. \quad (80)$$

To bound the total error, we apply the triangle inequality

$$\|\tilde{V}_{\text{II}} - F_{\text{II}}\| \leq \|\tilde{F}_{\text{II}} - F_{\text{II}}\| + \|\tilde{V}_{\text{II}} - \tilde{F}_{\text{II}}\| \quad (81)$$

The first term is determined by the truncation error. It has already been analyzed in [14] in the $\|\cdot\|_{\max}$ norm. We now derive an estimate for it in the $\|\cdot\|$ norm based on the following lemma.

Lemma 22. *Let $B, C \in \mathbb{C}^{N \times N}$. We have*

$$\|B \circ C\| \leq \sqrt{N} \|B\|_{\max} \|C\|. \quad (82)$$

Proof. Let e_1, \dots, e_N be the standard basis vectors in \mathbb{C}^N , and let $v = \sum_{i=1}^N v_i e_i$ be any vector. For each i , we have

$$\|(B \circ C)e_i\|_2 \leq \|B\|_{\max} \|Ce_i\|_2 \leq \|B\|_{\max} \|C\| \quad (83)$$

because $(B \circ C)e_i$ is obtained from Ce_i by multiplying each entry by a scalar of magnitude at most $\|B\|_{\max}$. By linearity and the triangle inequality, we have

$$\|(B \circ C)v\|_2 = \left\| \sum_{i=1}^N v_i (B \circ C)e_i \right\|_2 \leq \sum_{i=1}^N |v_i| \|(B \circ C)e_i\|_2 \leq \|B\|_{\max} \|C\| \|v\|_1. \quad (84)$$

Since $\|v\|_1 \leq \sqrt{N} \|v\|_2$, we obtain

$$\|(B \circ C)v\|_2 \leq \sqrt{N} \|B\|_{\max} \|C\| \|v\|_2 \quad (85)$$

for all $v \in \mathbb{C}^N$. The claim follows. \square

We can use Lemma 22 to compute an upper bound on K . This is carried out in Theorem 25 below. Next, we bound the second term in Equation (81), which will be used to determine the values of m and p in Theorem 25. We assume that the block-encoding of $M_{\vec{s}}$ is exact. This assumption is justified because we have black-box access to the oracle O_r , and the oracles O_c and O_A (Lemma 19) are constructed exactly. Furthermore, we assume that the quantum Fourier transform is implemented exactly, as we analyze the algorithm within the fault-tolerant regime. Define the normalization factors as $\alpha_{\vec{u}_r} = \|\vec{a}'_r\|_1$ and $\alpha_{\vec{v}_r} = 1$, where \vec{a}'_r are the coefficients appearing in Equation (47). The analysis in the previous section implies that $U_{\vec{u}_r}$ and $U_{\vec{v}_r}$ are exact block-encodings.

$$U_{\vec{u}_r} = \begin{pmatrix} D_{\vec{u}_r} / \alpha_{\vec{u}_r} & * \\ * & * \end{pmatrix}, \quad U_{\vec{v}_r} = \begin{pmatrix} D_{\vec{v}_r} / \alpha_{\vec{v}_r} & * \\ * & * \end{pmatrix}. \quad (86)$$

Since the errors introduced above render the block-encodings inexact in the construction of \tilde{V}_{II} , let $\tilde{U}_{\vec{u}_r}$ and $\tilde{U}_{\vec{v}_r}$ be the implemented block-encodings such that

$$\tilde{U}_{\vec{u}_r} = \begin{pmatrix} \tilde{D}_{\vec{u}_r} / \alpha_{\vec{u}_r} & * \\ * & * \end{pmatrix}, \quad \tilde{U}_{\vec{v}_r} = \begin{pmatrix} \tilde{D}_{\vec{v}_r} / \alpha_{\vec{v}_r} & * \\ * & * \end{pmatrix}, \quad (87)$$

with $\tilde{D}_{\vec{u}_r}$ and $\tilde{D}_{\vec{v}_r}$ obtained via finite-precision oracle access and approximate function evaluation. Let \tilde{F} and $\tilde{M}_{\vec{s}}$ denote the corresponding exact block-encodings of F and $M_{\vec{s}}$, respectively. Note that \tilde{V}_{II} can be written as

$$\tilde{V}_{\text{II}} = \sum_{r=0}^{K-1} \tilde{D}_{\vec{u}_r} \tilde{F} \tilde{M}_{\vec{s}} \tilde{D}_{\vec{v}_r}. \quad (88)$$

The normalization factor $1/\alpha$, defined in Equation (74), is omitted in the following analysis, as it affects only the post-selection success probability. We bound the unitary circuit synthesis error of the unnormalized top-left block in order to determine the required parameters (K, m, p) as functions of the target precision. We have

$$\|\tilde{V}_{\text{II}} - \tilde{F}_{\text{II}}\| = \left\| \sum_{r=0}^{K-1} \tilde{D}_{\vec{u}_r} \tilde{F} \tilde{M}_{\vec{s}} \tilde{D}_{\vec{v}_r} - \sum_{r=0}^{K-1} D_{\vec{u}_r} F M_{\vec{s}} D_{\vec{v}_r} \right\|, \quad (89)$$

$$\leq \sum_{r=0}^{K-1} \|(\tilde{D}_{\vec{u}_r} - D_{\vec{u}_r}) \tilde{F} \tilde{M}_{\vec{s}} \tilde{D}_{\vec{v}_r}\| + \sum_{r=0}^{K-1} \|D_{\vec{u}_r} F M_{\vec{s}} (\tilde{D}_{\vec{v}_r} - D_{\vec{v}_r})\|. \quad (90)$$

Here, the terms involving $\tilde{F} - F$ and $\tilde{M}_{\vec{s}} - M_{\vec{s}}$ vanish because we assume that $\|\tilde{M}_{\vec{s}} - M_{\vec{s}}\| = 0 = \|\tilde{F} - F\|$. Note that $\|F\| = \|\tilde{F}\| = 1$, $\|M_{\vec{s}}\| = \|\tilde{M}_{\vec{s}}\| = \sqrt{\|\vec{c}_s\|_\infty}$, $\|D_{\vec{u}_r}\| \leq \|\vec{\alpha}'_r\|_1$ and $\|D_{\vec{v}_r}\| \leq 1$. Hence, we have

$$\|\tilde{V}_{\text{II}} - \tilde{F}_{\text{II}}\| \leq \sqrt{\|\vec{c}_s\|_\infty} \sum_{r=0}^{K-1} \left(\|\tilde{D}_{\vec{u}_r} - D_{\vec{u}_r}\| + \|\vec{\alpha}'_r\|_1 \|\tilde{D}_{\vec{v}_r} - D_{\vec{v}_r}\| \right). \quad (91)$$

Since we have

$$\|D_{\vec{v}_r} - \tilde{D}_{\vec{v}_r}\| = \max_j |(\vec{v}_r)_j - (\tilde{v}_r)_j|, \quad \|D_{\vec{u}_r} - \tilde{D}_{\vec{u}_r}\| = \max_j |(\vec{u}_r)_j - (\tilde{u}_r)_j|, \quad (92)$$

it suffices to bound the worst-case scalar error in a single diagonal entry. We first compute the error in the evaluation of the complex exponential and the Chebyshev polynomials, which will allow us to determine the worst-case scalar error in a single diagonal entry. We first bound the complex exponential term. In what follows, we assume that $m \geq n+1$. In this case, the oracle constructing s_j is exact; hence, the only source of error is in t_j .

Lemma 23. *Let $m, n \in \mathbb{N}$ such that $m \geq n+1$ and $N = 2^n$. Let $y_j = t_j - s_j/N$ for $j = 0, \dots, N-1$, where t_j and s_j are provided by m -bit precision oracles. Let \tilde{y}_j denote the m -bit approximation of y_j . The errors in the complex exponential satisfy*

$$|e^{-i\pi N y_j} - e^{-i\pi N \tilde{y}_j}| \leq \pi N 2^{-m+1} \quad (93)$$

uniformly in j .

Proof. We have $|t_j - \tilde{t}_j| \leq 2^{-m}$. Hence, we have

$$|e^{-i\pi N y_j} - e^{-i\pi N \tilde{y}_j}| = \left| e^{-i\pi N(t_j - s_j/N)} - e^{-i\pi N(\tilde{t}_j - s_j/N)} \right| \quad (94)$$

$$\leq \pi N |(t_j - s_j/N) - (\tilde{t}_j - s_j/N)| \leq \pi N 2^{-m} \quad (95)$$

uniformly in j . \square

We now bound the error in the Chebyshev polynomials. Note that the Chebyshev polynomials are evaluated at two inputs, $x_j := 2j/N - 1$ and $y_j := (t_j - s_j/N)$. Since $j = 0, \dots, N-1$, the values $2j/N - 1$ can be computed exactly (see Proposition 9), as we use at least n qubits. On the other hand, there is an approximation error in computing $t_j - s_j/N$ via the oracles. Hence, we treat these cases separately below. In Lemma 24, we continue to denote $y_j = 2N(t_j - \frac{s_j}{N})$ for simplicity.

Lemma 24. Let $m, n \in \mathbb{N}$ such that $m \geq n + 1$. Let $q \leq K$ and $j = 0, \dots, N - 1$. Let $T_q(y_j) = \cos(q \arccos(y_j))$ denote the degree- q Chebyshev polynomial of the first kind. The errors in computing the Chebyshev polynomials can be bounded as follows:

(1) For $x_j = 2j/N - 1$, the error in the QSP implementation due to p -bit finite-precision evaluation of $\arccos(x)$ satisfies

$$|T_q(x_j) - \tilde{T}_q(x_j)| \leq q2^{-p+1} \leq K2^{-p+1}, \quad (96)$$

uniformly in j .

(2) For $y_j = 2N(t_j - s_j/N)$, where t_j and s_j are provided by m -bit precision oracles, let \tilde{y}_j denote the m -bit approximation. Let $y_j^* \in (\min(y_j, \tilde{y}_j), \max(y_j, \tilde{y}_j))$. The total Chebyshev polynomial error satisfies

$$|T_q(y_j) - \tilde{T}_q(y_j)| \leq q \left(2^{-p+1} + \frac{N2^{-m+1}}{\sqrt{1 - (y_j^*)^2}} \right) \leq K \left(2^{-p+1} + \frac{N2^{-m+1}}{\sqrt{1 - (y_j^*)^2}} \right). \quad (97)$$

Proof. Let $\theta_j = \arccos(\cdot)$, where the argument is either x_j or y_j , and define $\delta_{\theta_j} := |\theta_j - \tilde{\theta}_j|$.

(1) Let $x_j = 2j/N - 1$. The only source of error is the finite-precision evaluation of $\arccos(x_j)$ to p bits, giving a rotation-angle error $\delta_{\theta_j} \leq 2^{-p+1}$. By the mean-value theorem for the cosine function, the Chebyshev polynomial error is bounded by

$$|T_q(x_j) - \tilde{T}_q(x_j)| = |\cos(q\theta_j) - \cos(q(\theta_j + \delta_{\theta_j}))| \leq q\delta_{\theta_j} \leq q2^{-p+1} \leq K2^{-p+1}. \quad (98)$$

(2) Let $y_j = 2N(t_j - s_j/N)$, where t_j and s_j/N are provided by an m -bit precision oracle. We have $|y_j - \tilde{y}_j| \leq 2N2^{-m} = N2^{-m+1}$. The rotation angle is $\theta_j = \arccos(y_j)$, while the computed rotation is $\tilde{\theta}_j$ with finite-precision p -bit evaluation. Applying the mean-value theorem to \arccos , there exists $y_j^* \in (\min(y_j, \tilde{y}_j), \max(y_j, \tilde{y}_j))$ such that

$$|\theta_j - \arccos(\tilde{y}_j)| \leq \frac{|y_j - \tilde{y}_j|}{\sqrt{1 - (y_j^*)^2}} \leq \frac{N2^{-m+1}}{\sqrt{1 - (y_j^*)^2}}. \quad (99)$$

Let $\tilde{\theta}_j = \arccos(\tilde{y}_j)$. By the triangle inequality, we have

$$\delta_{\theta_j} = |\theta_j - \tilde{\theta}_j| \leq |\theta_j - \arccos(\tilde{y}_j)| + |\arccos(\tilde{y}_j) - \tilde{\theta}_j| \leq \frac{N2^{-m+1}}{\sqrt{1 - (y_j^*)^2}} + 2^{-p+1}, \quad (100)$$

Applying the mean-value theorem to the cosine function,

$$|T_q(y_j) - \tilde{T}_q(y_j)| = |\cos(q\theta_j) - \cos(q\tilde{\theta}_j)| \leq q\delta_{\theta_j} = q \left(2^{-p+1} + \frac{N2^{-m+1}}{\sqrt{1 - (y_j^*)^2}} \right). \quad (101)$$

Since the maximum Chebyshev degree in the truncated expansion is $q \leq K$, the error is bounded by

$$|T_q(y_j) - \tilde{T}_q(y_j)| \leq K \left(2^{-p+1} + \frac{N2^{-m+1}}{\sqrt{1 - (y_j^*)^2}} \right). \quad (102)$$

This completes the proof. \square

We can now compute $\|D_{\vec{v}_r} - \tilde{D}_{\vec{v}_r}\|$ and $\|D_{\vec{u}_r} - \tilde{D}_{\vec{u}_r}\|$. Using Lemma 24, we have

$$\|D_{\vec{v}_r} - \tilde{D}_{\vec{v}_r}\| \leq \begin{cases} 0, & r = 0, \\ r2^{-p+1}, & r \geq 1, \end{cases} \quad (103)$$

Similarly, using Lemma 23, and Lemma 24, we have

$$\|D_{\vec{u}_r} - \tilde{D}_{\vec{u}_r}\| \leq \|\vec{\alpha}'_r\|_1 \left(\pi N 2^{-m} + K \left(2^{-p+1} + \max_j \frac{N 2^{-m+1}}{\sqrt{1 - (y_j^*)^2}} \right) \right), \quad (104)$$

Let $\alpha' = \sum_{r=0}^{K-1} \|\vec{\alpha}'_r\|_1$. Substituting the bounds in Equation (91), we have

$$\|\tilde{V}_{\text{II}} - \tilde{F}_{\text{II}}\| \leq \sqrt{\|\vec{c}_s\|_\infty} \sum_{r=0}^{K-1} \|\vec{\alpha}'_r\|_1 \left(\pi N 2^{-m} + K 2^{-p+1} + \max_j \frac{N K 2^{-m+1}}{\sqrt{1 - (y_j^*)^2}} + K 2^{-p+1} \right), \quad (105)$$

$$= \alpha' \sqrt{\|\vec{c}_s\|_\infty} \left(\pi N 2^{-m} + K 2^{-p+2} + \max_j \frac{N K 2^{-m+1}}{\sqrt{1 - (y_j^*)^2}} \right). \quad (106)$$

We can now complete our error analysis by specifying the parameters (K, m, p) so that the total error remains below the prescribed tolerance ϵ .

Theorem 25. *Let $\epsilon > 0$ and let $n, m, p, K \in \mathbb{N}$ with $m \geq n + 1$ and $N = 2^n$. Let $\tilde{V}_{\text{II}} = \sum_{r=0}^{K-1} \tilde{D}_{\vec{u}_r} \tilde{F} \tilde{M}_{\vec{s}} \tilde{D}_{\vec{v}_r}$ denote the quantum implementation of the Type-II non-uniform quantum Fourier transform with Chebyshev truncation degree K , m -bit oracle precision, and p -bit finite-precision evaluation of $\arccos(x)$ in the QSP implementation. Let $\|\vec{\alpha}'_r\|_1 = \sum_{q=0}^{K-1} |\alpha'_{qr}|$, where α'_{qr} is defined in Equation (34). Define*

$$\alpha' = \sum_{r=0}^{K-1} \|\vec{\alpha}'_r\|_1, \quad y_j = 2N(t_j - s_j/N), \quad y_j^* \in (\min(y_j, \tilde{y}_j), \max(y_j, \tilde{y}_j)), \quad (107)$$

where \tilde{y}_j is a m -bit approximation of y_j . If (K, m, p) are chosen such that

$$K = \mathcal{O} \left(\frac{\log(\sqrt{N\|\vec{c}_s\|_\infty}/\epsilon)}{\log \log(\sqrt{N\|\vec{c}_s\|_\infty}/\epsilon)} \right), \quad (108)$$

$$m = \left\lceil \log_2 \frac{8\alpha' \sqrt{\|\vec{c}_s\|_\infty} (\pi N + K \max_j (1 - (y_j^*))^{-1/2}}{\epsilon} \right\rceil, \quad (109)$$

$$p = \left\lceil \log_2 \frac{16\alpha' \sqrt{\|\vec{c}_s\|_\infty} K}{\epsilon} \right\rceil, \quad (110)$$

then the total error of the quantum algorithm satisfies

$$\|\tilde{V}_{\text{II}} - F_{\text{II}}\| \leq \epsilon. \quad (111)$$

In particular, it suffices to choose m and p such that

$$m = \mathcal{O} \left(\log \left(\frac{K \sqrt{\|\vec{c}_s\|_\infty} (N + K \max_j (1 - (y_j^*))^{-1/2}}{\epsilon} \right) \right), \quad (112)$$

$$p = \mathcal{O} \left(\log \left(\frac{\sqrt{\|\vec{c}_s\|_\infty} K^2}{\epsilon} \right) \right). \quad (113)$$

Proof. We have

$$\|\tilde{V}_{\text{II}} - F_{\text{II}}\| \leq \underbrace{\|\tilde{F}_{\text{II}} - F_{\text{II}}\|}_{\text{truncation error}} + \underbrace{\|\tilde{V}_{\text{II}} - \tilde{F}_{\text{II}}\|}_{\text{block-encoding error}}, \quad (114)$$

where the first term is the Chebyshev truncation error and the second term is the block-encoding error. Using Lemma 22, the first term in Equation (81) can be expressed as

$$\|\tilde{F}_{\text{II}} - F_{\text{II}}\| = \|(A - A_K) \circ (FM_{\vec{s}})\| \quad (115)$$

$$\leq \sqrt{N} \|A - A_K\|_{\max} \|FM_{\vec{s}}\| \quad (116)$$

$$\leq \|\vec{c}_s\|_{\infty} \sqrt{N} \|A - A_K\|_{\max}. \quad (117)$$

The last equality follows since F is unitary, and we have

$$\|FM_{\vec{s}}\| = \|M_{\vec{s}}\| = \sqrt{\|\vec{c}_s\|_{\infty}}. \quad (118)$$

Hence, in order to ensure that $\|\tilde{F}_{\text{II}} - F_{\text{II}}\| \leq \epsilon/2$ for some $\epsilon > 0$, it suffices to choose $\epsilon'_{\text{trun}} = \epsilon/2\sqrt{N}\|\vec{c}_s\|_{\infty}$. Hence, it suffices to choose K such that

$$K = \mathcal{O}\left(\frac{\log(\sqrt{N}\|\vec{c}_s\|_{\infty}/\epsilon)}{\log\log(\sqrt{N}\|\vec{c}_s\|_{\infty}/\epsilon)}\right), \quad (119)$$

From (105), the block-encoding error satisfies

$$\|\tilde{V}_{\text{II}} - \tilde{F}_{\text{II}}\| \leq \alpha' \sqrt{\|\vec{c}_s\|_{\infty}} \left(\pi N 2^{-m} + K 2^{-p+2} + \max_j \frac{N K 2^{-m+1}}{\sqrt{1 - (y_j^*)^2}} \right). \quad (120)$$

Let $C := \alpha' \sqrt{\|\vec{c}_s\|_{\infty}}$ and $\kappa := \max_j \frac{1}{\sqrt{1 - (y_j^*)^2}}$. Using this notation, Equation (120) can be succinctly expressed as

$$\|\tilde{V}_{\text{II}} - \tilde{F}_{\text{II}}\| \leq C(2^{-m}(\pi N + 2N\kappa) + K 2^{-p+2}). \quad (121)$$

To ensure that the right-hand side is at most $\epsilon/2$, we can allocate the error budget equally between the oracle and QSP contributions, i.e.,

$$C 2^{-m}(\pi N + 2N\kappa) \leq \frac{\epsilon}{4}, \quad (122)$$

$$CK 2^{-p+2} \leq \frac{\epsilon}{4}. \quad (123)$$

Solving for m , we obtain

$$C 2^{-m}(\pi N + 2N\kappa) \leq \frac{\epsilon}{4} \iff m \geq \log_2 \left(\frac{4C(\pi N + 2N\kappa)}{\epsilon} \right). \quad (124)$$

Solving for p , we obtain

$$CK 2^{-p+2} \leq \frac{\epsilon}{4} \iff 2^{-p} \leq \frac{\epsilon}{16CK} \iff p \geq \log_2 \left(\frac{16CK}{\epsilon} \right). \quad (125)$$

Substituting the definitions of C and κ yields

$$m = \left\lceil \log_2 \left(\frac{4\alpha' \sqrt{\|\vec{c}_s\|_{\infty}} (\pi N + 2N\kappa) \max_j (1 - (y_j^*))^{-1/2}}{\epsilon} \right) \right\rceil, \quad (126)$$

$$p = \left\lceil \log_2 \left(\frac{16\alpha' \sqrt{\|\vec{c}_s\|_{\infty}} K}{\epsilon} \right) \right\rceil. \quad (127)$$

With these choices of m and p , the error satisfies $\|\tilde{V}_{\text{II}} - \tilde{F}_{\text{II}}\| \leq \epsilon$. Combined with the choice of K , we therefore have

$$\|\tilde{V}_{\text{II}} - F_{\text{II}}\| \leq \epsilon. \quad (128)$$

We now further simplify the choices of m and p . It is well known [56, 57] that for $\nu \geq 0$ and $0 \leq x \ll \nu$, we have

$$J_{\nu}(x) \sim \frac{(x/2)^{\nu}}{\Gamma(\nu + 1)}, \quad (129)$$

where Γ is the Gamma function. Furthermore, recall that $\alpha'_{qr} = \mathcal{O}(\alpha_{qr})$ (see Equation (34)), where α_{qr} is defined in Equation (33) with $\gamma = \frac{1}{2}$ by

$$\alpha_{qr} = \begin{cases} 4i^r J_{\frac{q+r}{2}}(-\pi/4) J_{\frac{r-q}{2}}(-\pi/4), & \text{if } \text{mod}(|q-r|, 2) = 0, \\ 0, & \text{otherwise} \end{cases} \quad (130)$$

The condition $\text{mod}(|q-r|, 2) = 0$ implies that q and r have the same parity. Hence, the order of the Bessel function J is an integer in Equation (130). Since we are interested in $|\alpha_{qr}|$, it suffices to evaluate the Bessel functions at $\pi/4$ and to assume $(r-q)/2 \geq 0$, as Bessel functions of integer order are either even or odd. Equation (129) now implies that $|\alpha_{qr}| = \mathcal{O}(1)$, since for the fixed value $x_0 = \pi/4$, the magnitude of $J_\nu(x_0)$ decreases rapidly as ν increases. Hence, $\alpha' = \mathcal{O}(K)$, since each of the K summands $|\alpha'_{qr}|$ is $\mathcal{O}(1)$. Based on Equation (126) and Equation (127), it suffices to choose m and p such that

$$m = \mathcal{O} \left(\log \left(\frac{NK\sqrt{\|\vec{c}_s\|_\infty}(1+K\max_j(1-(y_j^*))^{-1/2})}{\epsilon} \right) \right), \quad p = \mathcal{O} \left(\log \left(\frac{\sqrt{\|\vec{c}_s\|_\infty}K^2}{\epsilon} \right) \right). \quad (131)$$

This completes the proof. \square

The expressions in Theorem 25 are rather involved. Noting that $N = 2^n$ and $\|\vec{c}_s\|_\infty = \mathcal{O}(2^n)$, we can further simplify the $\mathcal{O}(\cdot)$ estimates in Theorem 25 in terms of n , ϵ , and $\kappa := \max_j \frac{1}{\sqrt{1-(y_j^*)^2}}$.

Noting that $\sqrt{N\|\vec{c}_s\|_\infty} = \mathcal{O}(2^n)$, we have

$$\log \left(\frac{\sqrt{N\|\vec{c}_s\|_\infty}}{\epsilon} \right) = \Theta(n) + \log \left(\frac{1}{\epsilon} \right) = \Theta \left(n + \log \left(\frac{1}{\epsilon} \right) \right). \quad (132)$$

Hence, we can simplify the complexity estimate for K in Equation (108) to

$$K = \mathcal{O} \left(\frac{n + \log(1/\epsilon)}{\log(n + \log(1/\epsilon))} \right) = \mathcal{O} \left(n + \log \left(\frac{1}{\epsilon} \right) \right). \quad (133)$$

Similarly, we obtain

$$p = \mathcal{O} (n + \log(1/\epsilon) + \log K), \quad (134)$$

$$= \mathcal{O} \left(n + \log \left(\frac{1}{\epsilon} \right) + \log \left(n + \log \left(\frac{1}{\epsilon} \right) \right) \right) = \mathcal{O} \left(n + \log \left(\frac{1}{\epsilon} \right) \right). \quad (135)$$

The second last equality follows since $\log K = \mathcal{O}(n + \log(1/\epsilon))$. In a similar manner, we obtain

$$m = \mathcal{O} \left(\log \left(\frac{NK\sqrt{\|\vec{c}_s\|_\infty}(1+K\kappa)}{\epsilon} \right) \right), \quad (136)$$

$$= \mathcal{O} \left(\log \left(\frac{K2^{3n/2}(1+K\kappa)}{\epsilon} \right) \right), \quad (137)$$

$$= \mathcal{O} \left(\log K + n + \log(1+K\kappa) + \log \left(\frac{1}{\epsilon} \right) \right) = \mathcal{O} \left(n + \log \left(\frac{1}{\epsilon} \right) + \log(1+K\kappa) \right). \quad (138)$$

Corollary 26. *Let $\epsilon > 0$ and let $n, m, p, K \in \mathbb{N}$ with $m \geq n + 1$. Let \tilde{V}_{II} , y_j and y_j^* be defined as in Theorem 25. If the parameters (K, m, p) are chosen such that*

$$K = p\mathcal{O} \left(n + \log \left(\frac{1}{\epsilon} \right) \right), \quad m = \mathcal{O} \left(n + \log \left(\frac{1}{\epsilon} \right) + \log(1+K\kappa) \right), \quad (139)$$

where $\kappa := \max_j \frac{1}{\sqrt{1-(y_j^*)^2}}$, then $\|\tilde{V}_{\text{II}} - F_{\text{II}}\| \leq \epsilon$.

Proof. This follows from Theorem 25 and the discussion above. \square

6. CONCLUSION

We have developed a quantum algorithm for implementing the Type-II non-uniform discrete Fourier transform (NUDFT), which can be straightforwardly extended to the Type-I and Type-III variants. Furthermore, we have provided a rigorous error analysis that identifies the dominant sources of approximation error and derives explicit upper bounds on their respective contributions. Our analysis demonstrates that the required computational resources scale logarithmically with the inverse of the target precision and polynomially with the number of qubits.

6.1. Future Directions. We discuss below several future research directions stemming from this work:

- (1) The proposed NUQFT algorithm assumes oracle access to the non-uniform sampling points (cf. Assumption 10) as well as to the corresponding inverse mapping (cf. Assumption 18). A fundamental direction for future work is to identify concrete computational settings in which such oracles can be realized efficiently on a quantum computer, either through explicit circuit constructions or via natural data-generation models in which the required access arises intrinsically.
- (2) The computational complexity of the algorithm depends on the parameter $\kappa = \max_j(1 - (y_j^*)^{-1/2})$, which can become large for highly non-uniform sampling distributions. Such growth directly impacts resource requirements and may limit achievable precision. An important direction for future research is therefore the development of techniques to control or mitigate this κ -dependence. Possible approaches include preconditioning strategies, adaptive reparametrizations of the sampling grid, or alternative factorizations that reduce sensitivity to extreme non-uniformity.
- (3) The current framework relies on Chebyshev polynomial approximations combined with quantum signal processing. Alternative approximation schemes—such as rational approximations, Fourier–Bessel expansions, or minimax polynomial constructions tailored to restricted domains—may offer improved constants or reduced ancilla requirements. Investigating how these approximation methods can be incorporated into QSP or the more general QSFT framework may lead to more efficient NUQFT implementations.
- (4) Beyond polynomial approximation techniques, another promising alternative is the classical *gridding* approach to the NUDFT [12]. In this methodology, non-uniform data are first convolved with a smooth, localized kernel—often a Gaussian—to spread each sample onto a nearby over-sampled uniform grid. A fast Fourier transform is then applied on this grid, followed by a deconvolution or interpolation step. Recent advances in block-encoding techniques for dense or full-rank kernel matrices [58] suggest that such *gridding* based methods may admit efficient quantum implementations.
- (5) The present analysis is carried out within a fault-tolerant quantum computing model, assuming exact implementations of the quantum Fourier transform and idealized oracle access. An important direction for future work is the explicit compilation of the NUQFT into fault-tolerant gate sets, with particular emphasis on optimizing resource metrics such as T -count and T -depth and adapting the construction to hardware constraints including limited qubit connectivity and restricted native gate sets. A complementary direction is to extend the analysis to near-term and intermediate-scale quantum devices by incorporating realistic noise models and error-mitigation strategies. In such settings, approximate quantum Fourier transform constructions that eliminate rotation gates with exponentially small angles (cf. Equation (54)) may substantially reduce circuit depth while maintaining sufficient accuracy for practical applications.
- (6) Many applications of non-uniform Fourier analysis arise in higher dimensions. Extending the NUQFT framework to multidimensional NUDFTs, for example through tensorized or separable low-rank factorizations, is therefore a natural direction for future research. More broadly, the

techniques developed in this work may be extended to other classes of non-uniform integral transforms, including non-uniform cosine transforms, non-uniform Laplace transforms, and related transformations such as the discrete Legendre transform and Fourier transforms defined on manifolds.

(7) Finally, the NUQFT is intended to serve as a subroutine within larger quantum algorithms rather than as a standalone primitive. An important direction for future work is to study its integration into end-to-end quantum pipelines, including state preparation, intermediate processing, and measurement and readout. Understanding how the NUQFT interacts with these surrounding components—and identifying application settings in which such integrated use is algorithmically effective or practically relevant—remains a significant and largely open problem.

REFERENCES

- [1] James W. Cooley and John W. Tukey. “An algorithm for the machine calculation of complex Fourier series”. In: *Mathematics of Computation* 19.90 (1965), pp. 297–301.
- [2] Li Tan and Jean Jiang. *Digital signal processing: fundamentals and applications*. Academic press, 2018.
- [3] Jie Shen, Tao Tang, and Li-Lian Wang. *Spectral methods: algorithms, analysis and applications*. Vol. 41. Springer Science & Business Media, 2011.
- [4] William L. Briggs and Van E. Henson. *The DFT: an owner’s manual for the discrete Fourier transform*. SIAM, 1995.
- [5] Sonali Bagchi and Sanjit K. Mitra. *The non-uniform discrete Fourier transform and its applications in signal processing*. Vol. 463. Springer Science & Business Media, 2012.
- [6] Chuan Qin, Chin-Chen Chang, and Pei-Ling Tsou. “Robust image hashing using non-uniform sampling in discrete Fourier domain”. In: *Digital Signal Processing* 23.2 (2013), pp. 578–585.
- [7] Qing Huo Liu, Xue Min Xu, Bo Tian, and Zhong Qing Zhang. “Applications of non-uniform fast transform algorithms in numerical solutions of differential and integral equations”. In: *IEEE Transactions on geoscience and remote sensing* 38.4 (2000), pp. 1551–1560.
- [8] Alok Dutt and Vladimir Rokhlin. “Fast Fourier transforms for non-equispaced data”. In: *SIAM Journal on Scientific computing* 14.6 (1993), pp. 1368–1393.
- [9] Antony F. Ware. “Fast approximate Fourier transforms for irregularly spaced data”. In: *SIAM Review* 40.4 (1998), pp. 838–856.
- [10] Daniel Potts, Gabriele Steidl, and Manfred Tasche. “Fast Fourier transforms for nonequispaced data: A tutorial”. In: *Modern Sampling Theory: Mathematics and Applications* (2001), pp. 247–270.
- [11] Jeffrey A. Fessler and Bradley P. Sutton. “Non-uniform fast Fourier transforms using min-max interpolation”. In: *IEEE transactions on signal processing* 51.2 (2003), pp. 560–574.
- [12] Leslie Greengard and June-Yub Lee. “Accelerating the non-uniform fast Fourier transform”. In: *SIAM review* 46.3 (2004), pp. 443–454.
- [13] June-Yub Lee and Leslie Greengard. “The type III non-uniform FFT and its applications”. In: *Journal of Computational Physics* 206.1 (2005), pp. 1–5.
- [14] Diego Ruiz-Antolin and Alex Townsend. “A non-uniform fast Fourier transform based on low rank approximation”. In: *SIAM Journal on Scientific Computing* 40.1 (2018), A529–A547.
- [15] Heather Wilber, Ethan N. Epperly, and Alex H. Barnett. “Superfast Direct Inversion of the Non-uniform Discrete Fourier Transform via Hierarchically Semiseparable Least Squares”. In: *SIAM Journal on Scientific Computing* 47.3 (2025), A1702–A1732.
- [16] Yingzhou Li and Jingyu Liu. *A Superfast Direct Solver for Type-III Inverse Nonuniform Discrete Fourier Transform*. 2025. arXiv: [2512.03733 \[math.NA\]](https://arxiv.org/abs/2512.03733).
- [17] Dan Coppersmith. *An approximate Fourier transform useful in quantum factoring*. 2002. arXiv: [quant-ph/0201067 \[quant-ph\]](https://arxiv.org/abs/quant-ph/0201067).

- [18] Michael A Nielsen and Isaac Chuang. *Quantum Computation and Quantum Information*. American Association of Physics Teachers, 2002.
- [19] Lin Lin. *Lecture Notes on Quantum Algorithms for Scientific Computation*. 2022. arXiv: [2201.08309 \[quant-ph\]](#).
- [20] Peter W. Shor. “Polynomial-time algorithms for prime factorization and discrete logarithms on a quantum computer”. In: *SIAM review* 41.2 (1999), pp. 303–332.
- [21] Alexei Y. Kitaev. *Quantum measurements and the Abelian Stabilizer Problem*. 1995. arXiv: [quant-ph/9511026 \[quant-ph\]](#).
- [22] Aram W. Harrow, Avinatan Hassidim, and Seth Lloyd. “Quantum algorithm for linear systems of equations”. In: *Physical review letters* 103.15 (2009), p. 150502.
- [23] Daniel S. Abrams and Seth Lloyd. “Quantum algorithm providing exponential speed increase for finding eigenvalues and eigenvectors”. In: *Physical Review Letters* 83.24 (1999), p. 5162.
- [24] Thomas G. Draper. *Addition on a Quantum Computer*. 2000. arXiv: [quant-ph/0008033 \[quant-ph\]](#).
- [25] Lidia Ruiz-Perez and Juan Carlos Garcia-Escartin. “Quantum arithmetic with the quantum Fourier transform”. In: *Quantum Information Processing* 16.6 (2017), p. 152.
- [26] Philipp Pfeffer. *Multidimensional Quantum Fourier Transformation*. 2023. arXiv: [2301.13835 \[quant-ph\]](#).
- [27] Yunseong Nam, Yuan Su, and Dmitri Maslov. “Approximate quantum Fourier transform with $O(n \log n)$ T gates”. In: *NPJ Quantum Information* 6.1 (2020), p. 26.
- [28] Elisa Bäumer, David Sutter, and Stefan Woerner. *Approximate Quantum Fourier Transform in Logarithmic Depth on a Line*. 2025. arXiv: [2504.20832 \[quant-ph\]](#).
- [29] Yuwei Jin, Xiangyu Gao, Minghao Guo, Henry Chen, Fei Hua, Chi Zhang, and Eddy Z. Zhang. “Optimizing quantum fourier transformation kernels for modern NISQ and FT architectures”. In: *SC24: International Conference for High Performance Computing, Networking, Storage and Analysis*. IEEE. 2024, pp. 1–15.
- [30] Berend Klaver, Stefan Rombouts, Michael Fellner, Anette Messinger, Kilian Ender, Katharina Ludwig, and Wolfgang Lechner. *SWAP-less Implementation of Quantum Algorithms*. 2024. arXiv: [2408.10907 \[quant-ph\]](#).
- [31] Hayato Goto. “Resource requirements for a fault-tolerant quantum Fourier transform”. In: *Physical Review A* 90.5 (2014), p. 052318.
- [32] Guang H. Low and Isaac L. Chuang. “Optimal Hamiltonian Simulation by Quantum Signal Processing”. In: *Physical Review Letters* 118.1 (Jan. 2017).
- [33] András Gilyén, Yuan Su, Guang H. Low, and Nathan Wiebe. “Quantum singular value transformation and beyond: exponential improvements for quantum matrix arithmetics”. In: *Proceedings of the 51st Annual ACM SIGACT Symposium on Theory of Computing*. STOC ’19. ACM, June 2019.
- [34] Andrew M. Childs and Nathan Wiebe. “Hamiltonian Simulation Using Linear Combinations of Unitary Operations”. In: *Quantum Information and Computation* 12 (2012), pp. 901–924.
- [35] Laszlo Gyongyosi and Sandor Imre. *An Improvement in Quantum Fourier Transform*. 2012. arXiv: [1207.4464 \[quant-ph\]](#).
- [36] Amir Fijany and Colin P. Williams. “Quantum wavelet transforms: Fast algorithms and complete circuits”. In: *NASA international conference on quantum computing and quantum communications*. Springer. 1998, pp. 10–33.
- [37] Mohsen Bagherimehrab and Alán Aspuru-Guzik. “Efficient quantum algorithm for all quantum wavelet transforms”. In: *Quantum Science and Technology* 9.3 (2024), p. 035010.
- [38] Julien Zylberman. *Fast Laplace transforms on quantum computers*. 2024. arXiv: [2412.05173 \[quant-ph\]](#).

[39] Akash Kumar Singh, Ashish Kumar Patra, Anurag K. S. V., Sai Shankar P., Ruchika Bhat, and Jaiganesh G. *A Polylogarithmic-Time Quantum Algorithm for the Laplace Transform*. 2025. arXiv: [2512.17980 \[quant-ph\]](#).

[40] Nitin Jha and Abhishek Parakh. *Quantum Hilbert Transform*. 2025. arXiv: [2505.23581 \[quant-ph\]](#).

[41] Henry Zhang and Joseph Li. *Efficient Quantum Circuits for the Hilbert Transform*. 2026. arXiv: [2601.10876 \[quant-ph\]](#).

[42] Andreas Klappenecker and Martin Rötteler. “Discrete cosine transforms on quantum computers”. In: *Proceedings of the 2nd International Symposium on Image and Signal Processing and Analysis*. IEEE. 2001, pp. 464–468.

[43] Artyom M. Grigoryan, Alexis A. Gomez, and Sos S. Agaian. “New method of computing the quantum cosine transforms”. In: *Multimodal Image Exploitation and Learning 2025*. Vol. 13457. SPIE. 2025, pp. 93–102.

[44] Chelsea A. Williams, Annie E. Paine, Hsin-Yu Wu, Vincent E. Elfving, and Oleksandr Kyriienko. *Quantum Chebyshev Transform: Mapping, Embedding, Learning and Sampling Distributions*. 2023. arXiv: [2306.17026 \[quant-ph\]](#).

[45] Siddhartha Jain, Vishnu Iyer, Rolando D. Somma, Ning Bao, and Stephen P. Jordan. *Efficient Quantum Hermite Transform*. 2025. arXiv: [2510.04929 \[quant-ph\]](#).

[46] Steven A. Cuccaro, Thomas G. Draper, Samuel A. Kutin, and David P. Moulton. *A new quantum ripple-carry addition circuit*. 2004. arXiv: [quant-ph/0410184 \[quant-ph\]](#).

[47] Thomas G. Draper, Samuel A. Kutin, Eric M. Rains, and Krysta M. Svore. “A logarithmic-depth quantum carry-lookahead adder”. In: *Quantum Information and Computation* 6.4 (July 2006), pp. 351–369.

[48] Alex Parent, Martin Roetteler, and Michele Mosca. *Improved reversible and quantum circuits for Karatsuba-based integer multiplication*. 2017. arXiv: [1706.03419 \[quant-ph\]](#).

[49] Craig Gidney. *Asymptotically Efficient Quantum Karatsuba Multiplication*. 2019. arXiv: [1904.07356 \[quant-ph\]](#).

[50] Mehdi Ramezani, Morteza Nikaeen, Farnaz Farman, Seyed Mahmoud Ashrafi, and Alireza Bahrampour. “Quantum multiplication algorithm based on the convolution theorem”. In: *Physical Review A* 108.5 (2023), p. 052405.

[51] Iain Burge, Michel Barbeau, and Joaquin Garcia-Alfaro. *Quantum CORDIC – Arcsin on a Budget*. 2024. arXiv: [2411.14434 \[quant-ph\]](#).

[52] Junaid Aftab and Haizhao Yang. “Approximating Korobov functions via quantum circuits”. In: *Communications in Mathematical Sciences* 23.8 (2025), pp. 2077–2101.

[53] Junaid Aftab, Christoph Schwab, Haizhao Yang, and Jakob Zech. *Quantum Circuit Encodings of Polynomial Chaos Expansions*. Submitted to *Quantum*. 2025. arXiv: [2506.01811 \[math.NA\]](#).

[54] Andrew M. Childs and Nathan Wiebe. “Hamiltonian Simulation Using Linear Combinations of Unitary Operations”. In: *Quantum Information and Computation* 12 (2012), pp. 901–924.

[55] Adenilton J. da Silva and Daniel K. Park. “Linear-depth quantum circuits for multiqubit controlled gates”. In: *Phys. Rev. A* 106 (4 Oct. 2022), p. 042602.

[56] George N. Watson. *A treatise on the theory of Bessel functions*. The University Press, 1922.

[57] Milton Abramowitz and Irene A. Stegun. *Handbook of Mathematical Functions*. US Government Printing Office, 1964.

[58] Quynh T. Nguyen, Bobak T. Kiani, and Seth Lloyd. “Block-encoding dense and full-rank kernels using hierarchical matrices: applications in quantum numerical linear algebra”. In: *Quantum* 6 (2022), p. 876.

DEPARTMENT OF MATHEMATICS, UNIVERSITY OF MARYLAND, COLLEGE PARK, MD 20742, USA
Email address: `junaida@umd.edu`

DEPARTMENT OF STATISTICS, UNIVERSITY OF CHICAGO, IL 60637, USA
Email address: `yuehaw.khoo@uchicago.edu`

DEPARTMENTS OF MATHEMATICS AND COMPUTER SCIENCE, UNIVERSITY OF MARYLAND, COLLEGE PARK, MD 20742, USA
Email address: `haizhao.yang@umd.edu`